High-Fidelity Flight Dynamic Analysis of Transonic Truss-Braced Wing

Nhan Nguyen*
NASA Ames Research Center, Moffett Field, CA 94035
Juntao Xiong†
KBR Wyle, Inc., Moffett Field, CA 94035

This paper presents a high-fidelity flight dynamic analysis of the Mach 0.8 Transonic Truss-Braced Wing (TTBW). Unsteady RANS CFD simulations of the Mach 0.8 TTBW in pitch, plunge, roll, and yaw oscillations are conducted in FUN3D. The time-domain data are transformed into the frequency-domain data by Fourier series. Transfer functions of the dynamic stability derivatives are then estimated by a frequency-domain regression. The dynamic stability derivatives with respect to the angle of attack are determined by the regression of the unsteady aerodynamic coefficients for the plunge motion. The dynamic stability derivatives with respect to the pitch rate are determined by the regression of the differential unsteady aerodynamic coefficients for the pitch motion upon the removal of the angle of attack contribution by the plunge motion. Similarly, dynamic stability derivatives with respect to the angle of sideslip, roll rate, and yaw rates are determined from the frequency domain regression. The longitudinal and lateral-direction flight dynamic models of the Mach 0.8 TTBW are constructed from these dynamic stability derivatives. The eigenvalues of the aircraft modes are analyzed to determine the vehicle stability.

I. Introduction

Vehicle stability analysis is an important study to determine both static and dynamic stability of flight vehicles. A set of linearized flight dynamic equations of motion are established to predict the vehicle stability and its motion under applied aerodynamic forces and moments generated by flight control surfaces. Static stability of an aircraft depends on steady state stability derivatives such as C_{m_α} and C_{l_β}. Dynamic stability depends on a larger set of stability derivatives which include both steady state and dynamic stability derivatives. The partial derivatives of the aerodynamic coefficients with respect to the dynamic states of the aircraft are usually called dynamic derivatives such as $C_{L_{\dot{\alpha}}}$, C_{m_q}, and $C_{m_{\dot{q}}}$. The dynamic stability derivatives with respect to the angular rates generally can be computed by various analytical techniques. On the other hand, dynamic stability derivatives with respect to the time derivatives of the aircraft states are more difficult to established. These stability derivatives account for the time delay in the aerodynamic response of the aircraft which can be important. The steady state and dynamic stability derivatives can be estimated experimentally by stability-and-control (S&C) wind tunnel experiments or analytically by unsteady flow simulations.

Typically, steady state stability derivatives can be readily computed by analytical methods or low-order methods such as vortex-lattice methods. Dynamic stability derivatives, on the other hand, are much more difficult to estimate since these quantities depend on the dynamic motion of the aircraft which involves unsteady flow. The numerical estimation of dynamic stability derivatives is a current research topic. Recent work in this area can be found in many references.[1–3] Many of these technique do not seem to adequately capture the various terms of the dynamic stability derivatives. More importantly, the effects of the frequency response on the dynamic stability derivatives is not well addressed. Murman uses reduced-frequency approach to address the frequency response, but the approach lacks sufficient details to enable a systematic approach for determining the dynamic stability derivatives.[3]

A new method for estimating the dynamic stability derivatives in the frequency domain has been developed.[4] The approach addresses sufficiently the effects of the frequency response on the dynamic stability derivatives. Using

*Senior Research Scientist and Technical Group Lead of Advanced Control and Engineering Systems Group, Intelligent Systems Division, nhan.t.nguyen@nasa.gov
†Aerospace Engineer, Intelligent System Division, juntao.xiong@nasa.gov

unsteady RANS CFD simulation results, the time histories of the aerodynamic coefficients are converted in the frequency domain as a function of the reduced frequency. A frequency-domain transfer function is designed to capture both the steady state and dynamic derivatives. The transfer function is formulated based on the Theodorsen's theory.[5] A frequency-domain regression analysis is then performed to estimate the transfer function. The proposed method can estimate those dynamic stability derivatives that are usually not captured in many analyses but do exist in the Theodorsen's theory such as $C_{m_{\dot{q}}}$ due to the apparent mass effect.

The proposed method is applied to the Transonic Truss-Braced Wing (TTBW). The Subsonic Ultra Green Aircraft Research (SUGAR) Transonic Truss-Braced Wing aircraft concept is a Boeing-developed N+3 aircraft configuration funded by the NASA ARMD Advanced Air Transport Technologies (AATT) project.[6,7] The TTBW aircraft concept is designed to be aerodynamically efficient by employing a wing aspect ratio of about 19.55 which is significantly greater than those of cantilever wing transport configurations. For example, the latest Boeing 777-X is reported to have a wing aspect ratio of 11. Without structural bracing, the increase in the wing root bending moment would require a significant structural reinforcement which would lead to an increase in the structural weight that would offset the aerodynamic benefit of the high aspect ratio wing. Thus, the design of a truss-braced structure is a multidisciplinary design optimization process that strives to achieve a delicate balance between aerodynamic efficiency and structural efficiency. In the SUGAR configuration, the trade between the aerodynamic performance and structural design results in a truss-braced configuration with the wings braced at approximately mid-span by two main struts. In addition, two jury struts, one on each wing, provide the additional structural reinforcement. Two versions of the TTBW configurations are currently being developed by Boeing; a Mach 0.745 version and a Mach 0.8 version. Figure 1 is an illustration of the Mach 0.8 TTBW aircraft.

Figure 1. Boeing Mach 0.8 Transonic Truss-Braced Wing Aircraft Concept

In the previous work, dynamic stability derivatives of the Mach 0.8 TTBW with respect to the angle of attack and pitch rate have been estimated.[4] This paper presents the results of the estimation of the additional dynamic stability derivatives of the TTBW with respect to the axial airspeed, angle of sideslip, roll rate, and yaw rate. These results provide a complete set of dynamic stability derivatives for analyzing the flight dynamic stability of the Mach 0.8 TTBW. The flight dynamic stability provides the information on the vehicle stability which will be used to assess the stability and control of the Mach 0.8 TTBW.

II. Stability Derivative Estimation Method

Consider a pitch oscillation of an aircraft where the pitch angle θ varies sinusoidally at a given frequency ω

$$\theta = \bar{\theta} + \tilde{\theta} \tag{1}$$

$$\tilde{\theta} = \theta_0 \sin \omega t = \theta_0 \sin k\tau \tag{2}$$

where $\bar{\theta}$ is the mean pitch angle, $\tilde{\theta}$ is the oscillating pitch angle, $\tau = \dfrac{2V_\infty t}{c}$ is a non-dimensional time, V_∞ is the freestream airspeed, c is the airfoil chord, and k is the reduced frequency. The flight path angle γ is defined as

$$\gamma = \theta - \alpha \tag{3}$$

If the flight path angle γ is zero, then the pitch angle θ is equal to the angle of attack α. The pitch rate q is the time derivative of the pitch angle, i.e., $q = \dot{\theta}$ if the bank angle ϕ and heading angle ψ are zero. It should be noted that some references in the literature make the equivalency between $\dot{\theta}$ and $\dot{\alpha}$, but generally these time derivatives are not the same.

The effects of the angle of attack and pitch angle are not always equivalent. The angle of attack α is defined as

$$\alpha = \tan^{-1} \frac{w}{u} \tag{4}$$

where w is the vertical airspeed component and u is the axial airspeed component. For small angles of attack, $u \approx V_\infty$ and $w \approx \alpha V_\infty$. The vertical airspeed w, which is constant along the aircraft fuselage, can be determined by the change in the altitude. A change in the altitude creates a vertical airspeed which changes the angle of attack. When an aircraft is pitched about its center of gravity (CG), the pitch rate q creates a linearly varying vertical airspeed along the aircraft fuselage. This induced vertical airspeed causes changes in the aerodynamic lift and pitching moment in a different way than the changes in the vertical airspeed created by changes in the altitude. The horizontal tail plays a dominant role in the dynamic stability derivatives with respect to the pitch rate, whereas the wing contributes largely to the stability derivatives with respect to the angle of attack.

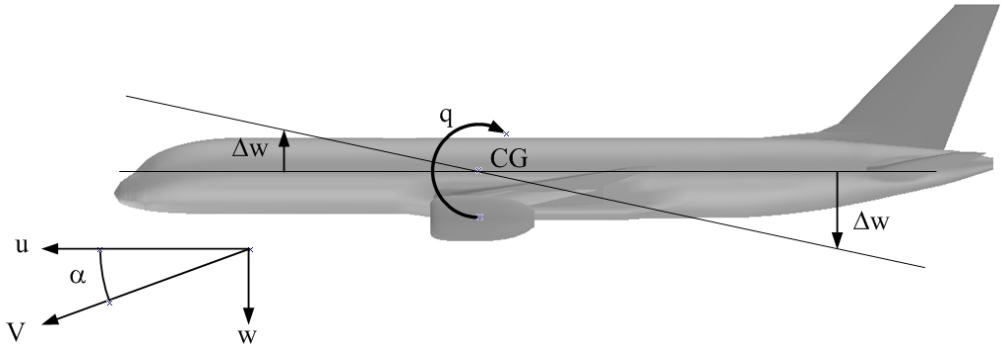

Figure 2. Effect of Pitch Rate on Aerodynamics

A. Frequency-Domain Formulation

The dynamic stability of an aircraft can be explained by the Theodorsen's theory which presents an analytical method for determining the lift and pitching moment of an airfoil in pitch oscillations in incompressible flow. The unsteady lift coefficient $\tilde{c}_l$ is established by the Theodorsen's theory as

$$\tilde{c}_l = c_{l_c} + c_{l_{nc}} \tag{5}$$

where c_{l_c} is the so-called circulatory lift coefficient and $c_{l_{nc}}$ is the so-called noncirculatory lift coefficient. The circulatory lift coefficient c_{l_c} is given by

$$c_{l_c} = c_{l_\alpha} C(k) \left(\tilde{\theta} + e_c \frac{\dot{\theta}}{V_\infty} \right) = c_{l_\alpha} C(k) \left(\tilde{\theta} + 2 \frac{e_c}{c} \tilde{q} \right) \tag{6}$$

where $\tilde{q} = \dfrac{d\theta}{d\tau} = \dfrac{cq}{2V_\infty}$ is the nondimensional pitch rate, c_{l_α} is the lift curve slope which is equal to 2π for incompressible flow, c is the chord length, and e_c is the distance from the pitch center to the three-quarter chord point which is positive when the pitch center lies forward of the three-quarter chord point. The complex-valued Theodorsen's function $C(k)$ is usually expressed as

$$C(k) = F(k) + iG(k) \tag{7}$$

The noncirculatory lift coefficient $c_{l_{nc}}$ is due to the inertial force acting on the oscillating airfoil and is given by

$$c_{l_{nc}} = c_{l_\alpha}\left(\frac{c\dot{\theta}}{4V_\infty} + \frac{e_m c\ddot{\theta}}{4V_\infty^2}\right) = c_{l_\alpha}\left(\frac{1}{2}\frac{d\theta}{d\tau} + \frac{e_m}{c}\frac{d\tilde{q}}{d\tau}\right) \tag{8}$$

where $\dfrac{d\tilde{q}}{d\tau} = \dfrac{d^2\theta}{d\tau^2} = \dfrac{c^2\dot{q}}{4V_\infty^2}$ is the nondimensional pitch acceleration due to the apparent mass effect and e_m is the distance from the pitch center to the mid-chord point, which is positive when the pitch center lies forward of the mid-chord point.

For zero flight path angle, $\tilde{\theta} = \tilde{\alpha}$. Thus, the unsteady lift coefficient $\tilde{c}_l$ can be expressed as

$$\tilde{c}_l = c_{l_\alpha}\left[C(k)\left(\tilde{\alpha} + 2\frac{e_c}{c}\tilde{q}\right) + \frac{1}{2}\tilde{q} + \frac{e_m}{c}\frac{d\tilde{q}}{d\tau}\right] \tag{9}$$

The unsteady pitching moment coefficient $\tilde{c}_m$ is treated by Theodorsen's theory in a similar manner where it is comprised of the circulatory and noncirculatory components and is given by

$$\tilde{c}_m = c_{l_\alpha}\left[C(k)\frac{e}{c}\left(\tilde{\alpha} + 2\frac{e_c}{c}\tilde{q}\right) - \frac{1}{2}\frac{e_c}{c}\tilde{q} - \left(\frac{1}{32} + \frac{e_m^2}{c^2}\right)\frac{d\tilde{q}}{d\tau}\right] \tag{10}$$

where e is the distance from the pitch center to the quarter-chord point which is positive when the pitch center lies aft of the quarter-chord point. The unsteady lift and pitching moment coefficient are therefore functions of the angle of attack, pitch rate, and pitch acceleration.

The motion of an airfoil in plunge is related to the pitching motion by the angle of attack

$$\tilde{\alpha} = \frac{\dot{h}}{V_\infty} \tag{11}$$

where $\dot{h} = w$ is the vertical airspeed which is positive in the downward direction as shown in Fig. 2.

The unsteady lift coefficient for an airfoil in plunge according to the Theodorsen's theory is expressed as

$$\tilde{c}_l = c_{l_\alpha}\left[C(k)\frac{\dot{h}}{V_\infty} + \frac{c\ddot{h}}{4V_\infty^2}\right] = c_{l_\alpha}\left[C(k)\,\tilde{\alpha} + \frac{1}{2}\frac{d\tilde{\alpha}}{d\tau}\right] \tag{12}$$

where $\dfrac{d\tilde{\alpha}}{d\tau} = \dfrac{c\dot{\alpha}}{2V_\infty}$ is the nondimensional angle of attack rate due to the apparent mass effect.

The pitching moment coefficient for an airfoil in plunge is given by

$$\tilde{c}_m = c_{l_\alpha}\left[C(k)\frac{e}{c}\tilde{\alpha} - \frac{1}{2}\frac{e_m}{c}\frac{d\tilde{\alpha}}{d\tau}\right] \tag{13}$$

To isolate the effect of pitch dynamics in the unsteady lift and pitching moment coefficient, the angle of attack contribution must be removed from Eqs. (9) and (10). This can be accomplished by subtracting the unsteady lift and pitching moment for the plunge motion from those for the pitch motion. The differences in the unsteady lift and pitching moment coefficients are expressed as

$$\Delta\tilde{c}_l = c_{l_\alpha}\left[C(k)2\frac{e_c}{c}\tilde{q} + \frac{1}{2}\tilde{q} + \frac{e_m}{c}\frac{d\tilde{q}}{d\tau} - \frac{1}{2}\frac{d\tilde{\alpha}}{d\tau}\right] \tag{14}$$

$$\Delta\tilde{c}_m = c_{l_\alpha}\left[C(k)2\frac{e}{c}\frac{e_c}{c}\tilde{q} - \frac{1}{2}\frac{e_c}{c}\tilde{q} - \left(\frac{1}{32} + \frac{e_m^2}{c^2}\right)\frac{d\tilde{q}}{d\tau} + \frac{1}{2}\frac{e_m}{c}\frac{d\tilde{\alpha}}{d\tau}\right] \tag{15}$$

Another type of dynamic stability derivatives is that due to the unsteady forward flight motion of an aircraft. This results in changes in the axial component of the aircraft velocity vector. The change in the axial airspeed u results in changes in the aerodynamic forces and moment. The effects of the axial airspeed can be complex if the flow is transonic. Using the Theodorsen's theory as a guide, the change in the axial airspeed results in a change in the effective angle of attack

$$\tilde{\alpha} = \frac{\bar{w}}{V_\infty + u} - \frac{\bar{w}}{V_\infty} \approx -\frac{\bar{w}}{V_\infty}\frac{u}{V_\infty} = -\bar{\alpha}\frac{u}{V_\infty} \tag{16}$$

The unsteady lift coefficient due to the change in the axial airspeed can be computed from the Theodorsen's theory for an airfoil in plunge as

$$\tilde{c}_l = -\bar{\alpha} c_{l_\alpha}(\tilde{u}) \left[C(k)\,\tilde{u} + \frac{1}{2}\frac{d\tilde{u}}{d\tau} \right] \tag{17}$$

where $\tilde{u} = \dfrac{u}{V_\infty}$ and $\dfrac{d\tilde{u}}{d\tau} = \dfrac{c\dot{u}}{2V_\infty^2}$ are nondimensional axial airspeed change and rate.

The lift curve slope $c_{l_\alpha}(\tilde{u})$ is generally a function of Mach number which in terms is a function of the axial airspeed change. Thus, the unsteady lift coefficient is nonlinear with respect to the axial airspeed. For small perturbations, the unsteady lift coefficient can be linearized to estimate the dynamic stability derivatives with respect to the axial speed. Linearization yields

$$\tilde{c}_l \approx -\bar{\alpha} \left(c_{l_\alpha} + \frac{\partial c_{l_\alpha}}{\partial \tilde{u}}\tilde{u} \right)\Bigg|_{\tilde{u}=0} \left[C(k)\,\tilde{u} + \frac{1}{2}\frac{d\tilde{u}}{d\tau} \right] \tag{18}$$

Therefore, the partial derivative of the unsteady lift coefficient with respect to the axial airspeed is evaluated as

$$\frac{\partial \tilde{c}_l}{\partial \tilde{u}} = -\bar{\alpha} c_{l_\alpha} C(k) - \bar{\alpha}\frac{\partial c_{l_\alpha}}{\partial \tilde{u}} \left[2C(k)\,\tilde{u} + \frac{1}{2}\frac{d\tilde{u}}{d\tau} \right] \tag{19}$$

Thus, generally, the partial derivative of the unsteady lift coefficient with respect to the axial airspeed is nonlinear. For small perturbations with $\tilde{u} \approx 0$, then

$$\frac{\partial \tilde{c}_l}{\partial \tilde{u}} \approx -\bar{\alpha} c_{l_\alpha} C(k) \tag{20}$$

For a general motion of an aircraft, we express the unsteady lift coefficient as

$$\tilde{C}_L = C_{L_{\tilde{u}}}(k)\,\tilde{u} + C_{L_{\dot{u}}}\frac{d\tilde{u}}{d\tau} + C_{L_{\tilde{\alpha}}}(k)\,\tilde{\alpha} + C_{L_{\dot{\alpha}}}\frac{d\tilde{\alpha}}{d\tau} + C_{L_{\tilde{q}}}(k)\,\tilde{q} + C_{L_{\dot{q}}}\frac{d\tilde{q}}{d\tau} \tag{21}$$

where the reduced frequency is based on the mean aerodynamic chord $\bar{c}$.

In the dimensional form, the unsteady lift coefficient is expressed as

$$\tilde{C}_L = C_{L_{\tilde{u}}}(k)\frac{u}{V_\infty} + C_{L_{\dot{u}}}\frac{\bar{c}\dot{u}}{2V_\infty^2} + C_{L_{\tilde{\alpha}}}(k)\,\tilde{\alpha} + C_{L_{\dot{\alpha}}}\frac{\bar{c}\dot{\alpha}}{2V_\infty} + C_{L_{\tilde{q}}}(k)\frac{\bar{c}q}{2V_\infty} + C_{L_{\dot{q}}}\frac{\bar{c}^2\dot{q}}{4V_\infty^2} \tag{22}$$

We note that the unsteady lift curve slope $C_{L_{\tilde{\alpha}}}(k)$ is a function of the reduced frequency and is equal to C_{L_α} only when $k = 0$. Thus, $C_{L_{\tilde{\alpha}}}(k)$ is a dynamic stability derivative whereas C_{L_α} is the steady state derivative when $k = 0$. Similarly, the dynamic stability derivative $C_{L_{\tilde{q}}}(k)$ gives C_{L_q} when $k = 0$, but C_{L_q} is considered a dynamic stability since the pitch rate is a dynamic state variable of an aircraft.

The unsteady pitching moment coefficient can be formulated the same way as

$$\tilde{C}_m = C_{m_{\tilde{u}}}(k)\frac{u}{V_\infty} + C_{m_{\dot{u}}}\frac{\bar{c}\dot{u}}{2V_\infty^2} + C_{m_{\tilde{\alpha}}}(k)\,\tilde{\alpha} + C_{m_{\dot{\alpha}}}\frac{\bar{c}\dot{\alpha}}{2V_\infty} + C_{m_{\tilde{q}}}(k)\frac{\bar{c}q}{2V_\infty} + C_{m_{\dot{q}}}\frac{\bar{c}^2\dot{q}}{4V_\infty^2} \tag{23}$$

In many low-fidelity aircraft flight dynamic stability analyses, the frequency dependency of the stability derivatives is usually ignored. While the dynamic stability derivatives $C_{L_{\dot{\alpha}}}$ and $C_{\dot{\alpha}}$ can be estimated by the Theodorsen's theory, the dynamic stability derivatives $C_{L_{\dot{q}}}$ and $C_{m_{\dot{q}}}$ are also usually ignored. In our work, the frequency dependency and the rate dynamic stability derivatives are fully captured.

In the current study, we will use the CFD simulation data for the plunge motion for the dynamic stability derivative estimation due to the angle of attack dynamics to remove the contributions of the angle of attack dynamics from the unsteady lift and pitching moment coefficients due to the pitch rate dynamics. This results in the components of

the unsteady lift and pitching moment coefficients that are only dependent on the pitch rate dynamics for use in the dynamic stability derivation estimation. These components are expressed as

$$\Delta\tilde{C}_L = C_{L_{\tilde{q}}}(k)\,\tilde{q} + C_{L_{\dot{\tilde{q}}}}\frac{d\tilde{q}}{d\tau} \tag{24}$$

$$\Delta\tilde{C}_m = C_{m_{\tilde{q}}}(k)\,\tilde{q} + C_{m_{\dot{\tilde{q}}}}\frac{d\tilde{q}}{d\tau} \tag{25}$$

The effects of the angle of sideslip β and yaw rate r on the unsteady aerodynamics due to the lateral airspeed component v can be treated in a similar manner as the effects of the angle of attack and pitch rate where the effects of the angle of sideslip and yaw rate is predominantly contributed by the vertical tail as opposed to the angle of attack contribution to the wing and horizontal tail. The unsteady aerodynamic analysis based on the Theodorsen's theory can then be carried in a similar manner. One distinct difference is that the angle of sideslip and yaw rate affect not only the side force coefficient C_Y and yawing moment C_n but also the rolling moment C_l. The unsteady motion in roll thus is coupled to the unsteady motion in yaw.

The angle of sideslip β contributes primarily to the unsteady side force coefficient generated by the vertical tail. The Theodorsen's theory for an airfoil in plunge can be used to estimate the unsteady side force and yawing moment coefficients as

$$\tilde{c}_Y = c_{Y_\beta}\left[C(k)\,\tilde{\beta} + \frac{1}{2}\frac{c}{b}\frac{d\tilde{\beta}}{d\tau}\right] \tag{26}$$

$$\tilde{c}_n = -c_{Y_\beta}\left[C(k)\,\frac{\bar{l}_v}{c}\tilde{\beta} + \frac{1}{2}\left(\frac{\bar{l}_v}{b} + \frac{1}{4}\frac{c}{b}\right)\frac{d\tilde{\beta}}{d\tau}\right] \tag{27}$$

where $\dfrac{d\tilde{\beta}}{d\tau} = \dfrac{b\dot{\beta}}{2V_\infty}$ is the nondimensional angle of sideslip rate, $\bar{l}_v$ is the distance from the aircraft CG to the one-quarter chord location on a vertical tail section and c is the chord of the vertical tail section.

The side force coefficient also generates a rolling moment coefficient as

$$\tilde{c}_l = \frac{z}{b}\tilde{c}_Y = \frac{z}{b}c_{Y_\beta}\left[C(k)\,\tilde{\beta} + \frac{1}{2}\frac{c}{b}\frac{d\tilde{\beta}}{d\tau}\right] \tag{28}$$

where z is the coordinate of the vertical tail section measured from the aircraft CG in the upward vertical direction. Note that $\tilde{c}_l$ here is the sectional rolling moment coefficient and should not be confused with the sectional lift coefficient.

Consider the effect of the yaw rate r on the vertical. The yaw rate creates an effective sideslip angle $\tilde{\beta}$

$$\tilde{\beta} = -\frac{l_v r}{V_\infty} = -\frac{l_v\dot{\psi}}{V_\infty} \tag{29}$$

where ψ is the yaw or heading angle and $l_v = \bar{l}_v + \dfrac{c}{2}$ is the distance from the aircraft CG to the three-quarter chord collocation point on a vertical tail section where the effective sidewash is placed.

The unsteady side force, yawing moment, and rolling moment coefficient due to the vertical contribution can be estimated using the Theodorsen's theory for an airfoil in pitch as

$$\tilde{c}_Y = -c_{Y_\psi}\left[C(k)\left(\tilde{\psi} + 2\frac{l_v}{b}\tilde{r}\right) + \frac{1}{2}\frac{c}{b}\tilde{r} + \frac{c}{b}\left(\frac{\bar{l}_v}{b} + \frac{1}{4}\frac{c}{b}\right)\frac{d\tilde{r}}{d\tau}\right] \tag{30}$$

$$\tilde{c}_n = c_{Y_\psi}\left\{C(k)\,\frac{\bar{l}_v}{c}\left(\tilde{\psi} + 2\frac{l_v}{b}\tilde{r}\right) + \frac{1}{2}\frac{l_v}{b}\tilde{r} + \left[\frac{c^2}{32b^2} + \left(\frac{\bar{l}_v}{b} + \frac{1}{4}\frac{c}{b}\right)^2\right]\frac{d\tilde{r}}{d\tau}\right\} \tag{31}$$

$$\tilde{c}_l = \frac{z}{b}\tilde{c}_Y = -\frac{z}{b}c_{Y_\psi}\left[C(k)\left(\tilde{\psi} + 2\frac{l_v}{b}\tilde{r}\right) + \frac{1}{2}\frac{c}{b}\tilde{r} + \frac{c}{b}\left(\frac{\bar{l}_v}{b} + \frac{1}{4}\frac{c}{b}\right)\frac{d\tilde{r}}{d\tau}\right] \tag{32}$$

where $\tilde{r} = \dfrac{d\psi}{d\tau} = \dfrac{br}{2V_\infty}$ and $\dfrac{d\tilde{r}}{d\tau} = \dfrac{d^2\psi}{d\tau^2} = \dfrac{b^2\dot{r}}{4V_\infty^2}$.

The effect of the roll rate p creates unsteady lift and drag on the wing and horizontal tail and unsteady side force on the vertical tail which in turn generates a rolling moment and yawing moment. The roll rate creates an effective angle of attack on a wing section equal to

$$\tilde{\alpha} = \frac{yp}{V_\infty} = \frac{y\dot{\phi}}{V_\infty} \tag{33}$$

where ϕ is the roll angle.

The angle of attack $\tilde{\alpha}$ creates a lift force which in turn generates a rolling moment. The unsteady rolling moment coefficient is computed as

$$\tilde{c}_l = -2\left(\frac{y}{b}\right)^2 c_{l_\alpha}\left[C(k)\,\tilde{p} + \frac{1}{2}\frac{c}{b}\frac{d\tilde{p}}{d\tau}\right] \tag{34}$$

where $\tilde{p} = \dfrac{d\phi}{d\tau} = \dfrac{bp}{2V_\infty}$, $\dfrac{d\tilde{p}}{d\tau} = \dfrac{d^2\phi}{d\tau^2} = \dfrac{b^2\dot{p}}{4V_\infty^2}$, and y is the coordinate of a wing section measured from the aircraft CG in the direction normal to the vertical plane pointing to the right wing.

The roll rate also creates an effective angle of sideslip on a vertical tail section equal to

$$\tilde{\beta} = \frac{zp}{V_\infty} \tag{35}$$

The unsteady angle of sideslip generates the unsteady side force, yawing moment, and rolling moment coefficients on the vertical tail are obtained as

$$\tilde{c}_Y = \frac{2z}{b}c_{Y_\beta}\left[C(k)\,\tilde{p} + \frac{1}{2}\frac{c}{b}\frac{d\tilde{p}}{d\tau}\right] \tag{36}$$

$$\tilde{c}_n = -2\frac{z}{b}c_{Y_\beta}\left[C(k)\,\frac{\bar{l}_v}{c}\tilde{p} + \frac{1}{2}\left(\frac{\bar{l}_v}{b} + \frac{1}{4}\frac{c}{b}\right)\frac{d\tilde{p}}{d\tau}\right] \tag{37}$$

$$\tilde{c}_l = 2\left(\frac{z}{b}\right)^2 c_{Y_\beta}\left[C(k)\,\tilde{p} + \frac{1}{2}\frac{c}{b}\frac{d\tilde{p}}{d\tau}\right] \tag{38}$$

For a general motion of an aircraft, we express the unsteady side force, rolling moment, and yawing coefficients as

$$\tilde{C}_Y = C_{Y_{\tilde{\beta}}}(k)\,\tilde{\beta} + C_{Y_{\dot{\beta}}}\frac{d\tilde{\beta}}{d\tau} + C_{Y_{\tilde{p}}}(k)\,\tilde{p} + C_{Y_{\dot{p}}}\frac{d\tilde{p}}{d\tau} + C_{Y_{\tilde{r}}}(k)\,\tilde{r} + C_{Y_{\dot{r}}}\frac{d\tilde{r}}{d\tau} \tag{39}$$

$$\tilde{C}_l = C_{l_{\tilde{\beta}}}(k)\,\tilde{\beta} + C_{l_{\dot{\beta}}}\frac{d\tilde{\beta}}{d\tau} + C_{l_{\tilde{p}}}(k)\,\tilde{p} + C_{l_{\dot{p}}}\frac{d\tilde{p}}{d\tau} + C_{l_{\tilde{r}}}(k)\,\tilde{r} + C_{l_{\dot{r}}}\frac{d\tilde{r}}{d\tau} \tag{40}$$

$$\tilde{C}_n = C_{n_{\tilde{\beta}}}(k)\,\tilde{\beta} + C_{n_{\dot{\beta}}}\frac{d\tilde{\beta}}{d\tau} + C_{n_{\tilde{p}}}(k)\,\tilde{p} + C_{n_{\dot{p}}}\frac{d\tilde{p}}{d\tau} + C_{n_{\tilde{r}}}(k)\,\tilde{r} + C_{n_{\dot{r}}}\frac{d\tilde{r}}{d\tau} \tag{41}$$

The contribution of the angle of sideslip to the unsteady side force, rolling, and yawing moment coefficients due to the yaw rate dynamics needs to be removed from the coefficients for the estimation of the dynamic stability derivatives in a similar manner as the treatment of the estimation of the dynamic stability derivatives with respect to the pitch rate.

B. Frequency-Domain Regression

The response of the unsteady lift coefficient of an aircraft to a sinusoidal plunge motion described by Eq. (2) is[4]

$$\tilde{C}_L = (U + iW)\,\tilde{\theta} = (U + iW)\,\theta_0 \sin k\tau \tag{42}$$

This is valid so long as the amplitude of the plunge motion is sufficiently small so that nonlinear aerodynamic effects become significant. The quantities U and W are the real part and imaginary part of the dynamic stability derivatives $C_{L_\alpha}(k)$ which can be computed from the Fourier series as

$$U(k) = \frac{k\int_0^{\frac{2n\pi}{k}} \tilde{C}_L \sin k\tau d\tau}{n\pi\theta_0} \tag{43}$$

$$W(k) = \frac{k\int_0^{\frac{2n\pi}{k}} \tilde{C}_L \cos k\tau d\tau}{n\pi\theta_0} \tag{44}$$

We express

$$\tilde{C}_L = C_{L_{\tilde{\alpha}}}(k)\,\tilde{\alpha} + b_1 \frac{d\alpha}{d\tau} \tag{45}$$

Let $\bar{s} = ik$ be the nondimensional Laplace variable, then we express

$$\tilde{C}_L = [H(\bar{s})\,c_0 + c_1\bar{s}]\,\tilde{\alpha} \tag{46}$$

where $H(\bar{s})$ is a unit magnitude transfer function such that

$$H(\bar{s})\,c_0 = C_{L_{\tilde{\alpha}}}(k) \tag{47}$$

Taking the partial derivative of $\tilde{C}_L$ with respect to $\tilde{\alpha}$, we obtain the transfer function from the angle of attack to the unsteady lift coefficient in the frequency domain

$$\frac{\partial C_L}{\partial \tilde{\alpha}}(\bar{s}) = H(\bar{s})\,c_0 + c_1\bar{s} \tag{48}$$

The unsteady pitching moment coefficient is analyzed in the same way as the lift coefficient and is expressed as

$$\frac{\partial C_m}{\partial \tilde{\alpha}}(\bar{s}) = G(\bar{s})\,d_0 + d_1\bar{s} \tag{49}$$

The transfer function $H(\bar{s})$ must have zero imaginary part at $\bar{s} = 0$ and also must be a stable and proper transfer function. From linear systems theory, a proper transfer function is expressed as a rational fraction with the polynomial in the numerator having a degree no greater than the degree of the polynomial in the denominator. A stable transfer function has stable poles which are the roots of the polynomial in the denominator. All stable poles must have negative real part.

The selection of the transfer function $H(\bar{s})$ is essential in the estimation of the dynamic stability derivatives. A good selection of $H(\bar{s})$ ensures a goodness of fit of the frequency response data in the frequency domain. The selection of the stable poles are also important. To ensure exponential decay in the response, the stable poles should be all negative real and not be complex as this will result in an amplification at the resonant frequency which is determined by the imaginary part of the poles. A general expression of the transfer function $H(\bar{s})$ is given by

$$H(\bar{s}) = 1 + \frac{\sum_{i=1}^{m} a_i \bar{s}^i}{\bar{s}^n + \sum_{i=0}^{n-1} b_i \bar{s}^i} \tag{50}$$

where $m \leq n$. The denominator polynomial is also expressed as

$$\bar{s}^n + \sum_{i=0}^{n-1} b_i \bar{s}^i = \Pi_{i=1}^{n}(\bar{s} - p_i) \tag{51}$$

where p_i is a pole such that $p_i < 0 \in \mathbb{R}$ for all $i = 1, \ldots, n$.

The simplest transfer function is a second-order transfer function

$$H(\bar{s}) = 1 + \frac{a_2\bar{s}^2 + a_1\bar{s}}{\bar{s}^2 + b_1\bar{s} + b_0} \tag{52}$$

In some instances, a higher-order transfer function may be necessary to provide a better regression of the frequency-domain data for complex flow in transonic regime. Transonic correction methods based on the Theodorsen's theory has been developed.[8–11] A frequency-domain regression is performed to compute the coefficients of the unsteady lift coefficient.

A frequency-domain regression is performed to compute the coefficients of the unsteady lift coefficient. The transfer function $\frac{\partial C_L}{\partial \tilde{\alpha}}(\bar{s})$ can be expressed as

$$\frac{\partial C_L}{\partial \tilde{\alpha}}(\bar{s}) = \frac{N(\bar{s})}{D(\bar{s})} \tag{53}$$

where $N(\bar{s})$ is a polynomial of degree $n+1$ and $D(\bar{s})$ is a polynomial of degree n. The poles are pre-selected to be negative real stable poles. Hence, the polynomial $D(\bar{s})$ is known. The objective of the regression is to estimate the polynomial coefficients of the polynomial $N(\bar{s})$. Assuming $m=n$ is even, the polynomials $N(\bar{s})$ and $D(\bar{s})$ are expressed as

$$\begin{aligned} N(\bar{s}) = \sum_{j=0}^{n+1} e_j \bar{s}^j &= \left[e_0 - e_2 k^2 + e_4 k^4 - \cdots + (-1)^{n/2} e_n k^n\right] + i\left[e_1 k - e_3 k^3 + e_5 k^5 - \cdots + (-1)^{n/2} e_{n+1} k^{n+1}\right] \\ &= \sum_{j=0}^{n/2} (-1)^j e_{2j} k^{2j} + i \sum_{j=0}^{n/2} (-1)^j e_{2j+1} k^{2j+1} \end{aligned} \tag{54}$$

$$\begin{aligned} D(\bar{s}) = \bar{s}^n + \sum_{j=0}^{n-1} b_j \bar{s}^j &= (-1)^{n/2} k^n + \left[b_0 - b_2 k^2 + b_4 k^4 - \cdots + (-1)^{n/2-1} b_{n-2} k^{n-2}\right] \\ &\quad + i\left[b_1 k - b_3 k^3 + b_5 k^5 - \cdots + (-1)^{n/2-1} b_{n-1} k^{n-1}\right] \\ &= (-1)^{n/2} k^n + \sum_{j=0}^{n/2-1} (-1)^j b_{2j} k^{2j} + i \sum_{j=0}^{n/2-1} (-1)^j b_{2j+1} k^{2j+1} \end{aligned} \tag{55}$$

The estimation error between the transfer function and the frequency domain data is expressed as

$$\Delta(\bar{s}) = \frac{\partial \tilde{C}_L}{\partial \tilde{\alpha}}(\bar{s}) - [U(k) + iW(k)] = \frac{N(\bar{s})}{D(\bar{s})} - [U(k) + iW(k)] \tag{56}$$

The estimation error goes to zero if the magnitude of the numerator of the estimation error is zero. We define an alternative estimation error

$$\varepsilon(\bar{s}) = D(\bar{s})\Delta(\bar{s}) = N(\bar{s}) - D(\bar{s})[U(k) + iW(k)] \tag{57}$$

$\varepsilon(\bar{s})$ is separated into the real part and imaginary part as

$$\varepsilon(\bar{s}) = \boldsymbol{\Theta}^\top [\boldsymbol{\Phi}_R(k) + i\boldsymbol{\Phi}_I(k)] - [y_R(k) + iy_I(k)] \tag{58}$$

where

$$\boldsymbol{\Theta} = \begin{bmatrix} e_{n+1} & e_n & \cdots & e_1 & e_0 \end{bmatrix}^\top \tag{59}$$

$$\boldsymbol{\Phi}_R(k) = \begin{bmatrix} 0 & (-1)^{n/2} k^n & \cdots & 0 & 1 \end{bmatrix}^\top \tag{60}$$

$$\boldsymbol{\Phi}_I(k) = \begin{bmatrix} (-1)^{n/2} k^{n+1} & 0 & \cdots & k & 0 \end{bmatrix}^\top \tag{61}$$

$$y_R(k) = \Re(D(k))U(k) - \Im(D(k))W(k) \tag{62}$$

$$y_I(k) = \Re(D(k))W(k) + \Im(D(k))U(k) \tag{63}$$

The estimation of the transfer function can be obtained by minimizing the magnitude square of the estimation error $\varepsilon(\bar{s})$ by the following cost function:

$$\begin{aligned} \min_{\boldsymbol{\Theta}} J &= \sum_{j=1}^{N} \frac{1}{2} \left\|\varepsilon(\bar{s}_j)\right\|^2 = \sum_{j=1}^{N} \frac{1}{2} \left\|\boldsymbol{\Theta}^\top \boldsymbol{\Phi}(k_j) - y(k_j)\right\|^2 \\ &= \sum_{j=1}^{N} \frac{1}{2} \left[\left\|\boldsymbol{\Theta}^\top \boldsymbol{\Phi}_R(k_j) - y_R(k_j)\right\|^2 + \left\|\boldsymbol{\Theta}^\top \boldsymbol{\Phi}_I(k_j) - y_I(k_j)\right\|^2\right] \end{aligned} \tag{64}$$

The estimation is performed over a data set of N data points. The standard method for minimization is to obtain the necessary condition and set it to zero. This results in

$$\frac{\partial J}{\partial \boldsymbol{\Theta}} = \sum_{j=1}^{N} \left\{\boldsymbol{\Phi}_R(k_j)\left[\boldsymbol{\Phi}_R^\top(k_j)\boldsymbol{\Theta} - y_R(k_j)\right] + \boldsymbol{\Phi}_I(k_j)\left[\boldsymbol{\Phi}_I^\top(k_j)\boldsymbol{\Theta} - y_I(k_j)\right]\right\} = \mathbf{0} \tag{65}$$

The resulting equations can be cast in a matrix equation of the form

$$\mathbf{A}\boldsymbol{\Theta} = \mathbf{b} \tag{66}$$

where

$$\mathbf{A} = \sum_{j=1}^{N} \left[\boldsymbol{\Phi}_R(k_j) \boldsymbol{\Phi}_R^{\top}(k_j) + \boldsymbol{\Phi}_I(k_j) \boldsymbol{\Phi}_I^{\top}(k_j) \right] \tag{67}$$

$$\mathbf{b} = \sum_{j=1}^{N} \left[\boldsymbol{\Phi}_R(k_j) y_R(k_j) + \boldsymbol{\Phi}_I(k_j) y_I(k_j) \right] \tag{68}$$

The pre-selected poles are chosen for the regression to satisfy the condition $|\max \mathbf{p}| \leq \max k$ where $\mathbf{p} = \begin{bmatrix} p_1 & \cdots & p_n \end{bmatrix}^{\top}$. This is to ensure that the poles are not unrealistically set too far outside the frequency bandwidth of the data. The poles can be optimized by an exhaustive search method with the values generated by a random function. This is essentially an outer loop optimization process which is defined by

$$\min_{\mathbf{p}_{i,i=1,\ldots M}} \min_{\boldsymbol{\Theta}} J = \sum_{j=1}^{N} \frac{1}{2} \left\| \boldsymbol{\Theta}^{\top} \boldsymbol{\Phi}(k_j) - y(k_j, \mathbf{p}_i) \right\|^2 \tag{69}$$

Once the coefficients e_j, $j = 1,\ldots,n+2$ and b_j, $j = 1,\ldots,n$ are determined, the coefficients a_i and c_i are determined next by solving a set of nonlinear equations that map the coefficients e_i and b_i to the coefficients a_i and c_i from the following equation:

$$\frac{\partial C_L}{\partial \tilde{\alpha}}(\bar{s}) = \left(1 + \frac{\sum_{i=1}^{n} a_i \bar{s}^i}{\bar{s}^n + \sum_{i=0}^{n-1} b_i \bar{s}^i} \right) c_0 + c_1 \bar{s} = \frac{\sum_{i=0}^{n+1} e_i \bar{s}^i}{\bar{s}^n + \sum_{i=0}^{n-1} b_i \bar{s}^i} \tag{70}$$

The solutions are given by

$$c_0 = \frac{e_0}{b_0} \tag{71}$$

$$c_1 = e_{n+1} \tag{72}$$

$$a_i = \begin{cases} \frac{e_i - b_{i-1} c_1}{c_0} - b_i & i = 1,\ldots,n-1 \\ \frac{e_i - b_{i-1} c_1}{c_0} - 1 & i = n \end{cases} \tag{73}$$

The dynamic stability derivative estimation for the pitch rate dynamics can be performed in the same manner using the components of the unsteady lift and pitching moment coefficients with the angle of attack contribution removed. The component of the unsteady lift coefficient with the angle of attack contribution removed is computed as

$$\Delta \tilde{C}_L = (T + iV) \tilde{\theta} - C_{L_{\tilde{\alpha}}}(k) \tilde{\theta} \tag{74}$$

where $T(k)$ and $V(k)$ are the Fourier sine and cosine series coefficients obtained from the component of the unsteady lift coefficient due to the pitch rate dynamics alone, and $C_{L_{\tilde{\alpha}}}(k)$ is the dynamic stability derivative obtained from the plunge motion as computed by Eq. (47). By subtracting off the angle of attack contribution from the unsteady lift coefficient due to the pitch rate dynamics, the remaining component of the unsteady lift coefficient $\Delta \tilde{C}_L$ is a function of the pitch rate only and therefore can be expressed as

$$\Delta \tilde{C}_L = (Q + iP) \frac{d\theta}{d\tau} \tag{75}$$

Equating Eq. (74) to Eq. (75), we obtain

$$Q = \frac{V - \Im(H(s)) c_0}{k} \tag{76}$$

$$P = \frac{-T + \Re(H(s)) c_0}{k} \tag{77}$$

Alternatively, the component of the unsteady lift coefficient without the angle of attack contribution can be computed by subtracting the unsteady lift coefficient for the plunge motion from that for the pitch motion. This is expressed as

$$\Delta\tilde{C}_L = (T+iV)\,\tilde{\alpha} - (U+iW)\,\tilde{\alpha} + C_{L_{\dot{\alpha}}}\bar{s}\tilde{\alpha} \tag{78}$$

where $C_{L_{\dot{\alpha}}}$, which is constant, is the dynamic stability derivative with respect to the angle of attack rate obtained from the plunge motion. Hence, we have

$$Q = \frac{V - W + kc_1}{k} \tag{79}$$

$$P = \frac{-T + U}{k} \tag{80}$$

C. Dynamic Stability Derivatives Due to Unsteady Drag Coefficient

Regarding the drag coefficient which is nonlinear with respect to the angle of attack, the unsteady drag coefficient is proposed to be modeled as a function of the unsteady lift coefficient according to the parabolic drag polar model

$$C_D = C_{D_0} + K(k)\left(\bar{C}_L + \tilde{C}_L\right)^2 \tag{81}$$

where $\bar{C}_L$ is the trim lift coefficient and $K(k)$ is a frequency dependent drag polar parameter.

Upon expansion, the unsteady drag coefficient is written as

$$C_D = \bar{C}_D + 2K(k)\bar{C}_L\tilde{C}_L + K(k)\tilde{C}_L^2 \tag{82}$$

where $\bar{C}_D$ is the trim drag coefficient.

The stability derivatives of the drag coefficient can be computed from CFD simulations by decomposing the response into a linear component and quadratic component. The unsteady drag coefficient is described by a quadratic relationship with the unsteady lift coefficient as

$$C_D = \bar{C}_D + (X_1 + iY_1)\,\tilde{C}_L + (X_2 + iY_2)\,\tilde{C}_L^2 \tag{83}$$

The quantity $\tilde{C}_L^2$ is expressed as

$$\begin{aligned}\tilde{C}_L^2 &= \left[(U+iW)\,\alpha_0 \sin k\tau\right]^2 = \left(U\alpha_0 \sin k\tau + W\alpha_0 \cos k\tau\right)^2 \\ &= \frac{1}{2}\left(U^2+W^2\right)\alpha_0^2 - \frac{1}{2}\left(U^2-W^2\right)\alpha_0^2 \cos 2k\tau + UW\alpha_0^2 \sin 2k\tau\end{aligned} \tag{84}$$

Removing the mean value from $\tilde{C}_L^2$, we write the unsteady drag coefficient as

$$\begin{aligned}\tilde{C}_D = {} & (X_1 + iY_1)\,(U+iW)\,\alpha_0 \sin k\tau \\ & + (X_2 + iY_2)\left[-\frac{1}{2}\left(U^2-W^2\right)\alpha_0^2 \cos 2k\tau + UW\alpha_0^2 \sin 2k\tau\right]\end{aligned} \tag{85}$$

The quantities X_1, X_2, Y_1, and Y_2 are evaluated as

$$X_1(k) = \frac{kU(k)\int_0^{\frac{2n\pi}{k}} \tilde{C}_D \sin k\tau d\tau + kW(k)\int_0^{\frac{2n\pi}{k}} \tilde{C}_D \cos k\tau d\tau}{n\pi\alpha_0\left[U^2(k) + W^2(k)\right]} \tag{86}$$

$$Y_1(k) = \frac{-kW(k)\int_0^{\frac{2n\pi}{k}} \tilde{C}_D \sin k\tau d\tau + kU(k)\int_0^{\frac{2n\pi}{k}} \tilde{C}_D \cos k\tau d\tau}{n\pi\alpha_0\left[U^2(k) + W^2(k)\right]} \tag{87}$$

$$X_2(k) = \frac{4kU(k)W(k)\int_0^{\frac{2n\pi}{k}} \tilde{C}_D \sin 2k\tau d\tau - 2k\left[U^2(k) - W^2(k)\right]\int_0^{\frac{2n\pi}{k}} \tilde{C}_D \cos 2k\tau d\tau}{n\pi\alpha_0^2\left[U^2(k) + W^2(k)\right]^2} \tag{88}$$

$$Y_2(k) = \frac{k\left[U^2(k) - W^2(k)\right]\int_0^{\frac{2n\pi}{k}} \tilde{C}_D \sin 2k\tau d\tau + 2kU(k)W(k)\int_0^{\frac{2n\pi}{k}} \tilde{C}_D \cos 2k\tau d\tau}{n\pi\alpha_0^2\left[U^2(k) + W^2(k)\right]^2} \tag{89}$$

To model the unsteady drag coefficient, we choose suitable proper transfer functions for the partial derivatives of $\tilde{C}_D$ with respect to $\tilde{C}_L$ and $\tilde{C}_L^2$ as

$$\frac{\partial \tilde{C}_D}{\partial \tilde{C}_L}(\bar{s}) = \frac{\sum_{i=0}^{n} f_i \bar{s}^i}{\bar{s}^n + \sum_{i=0}^{n-1} g_i \bar{s}^i} = X_1 + iY_1 \tag{90}$$

$$\frac{\partial \tilde{C}_D}{\partial \tilde{C}_L^2}(\bar{s}) = \frac{\sum_{i=0}^{n} u_i \bar{s}^i}{\bar{s}^n + \sum_{i=0}^{n-1} v_i \bar{s}^i} = X_2 + iY_2 \tag{91}$$

The transfer functions are then estimated by the frequency-domain regression in the same manner. The dynamic stability derivatives of the unsteady drag coefficient are then estimated from the dynamic stability derivatives of the unsteady lift coefficient by the following equation:

$$C_{D_{\tilde{\alpha}}}(k)\,\tilde{\alpha} + C_{D_{\dot{\alpha}}}(k)\frac{d\tilde{\alpha}}{d\tau} = \frac{\partial \tilde{C}_D}{\partial \tilde{C}_L}(\bar{s})\left[C_{L_{\tilde{\alpha}}}(k)\,\tilde{\alpha} + C_{L_{\dot{\alpha}}}\frac{d\tilde{\alpha}}{d\tau}\right] \tag{92}$$

The nonlinear dynamic stability derivatives of the unsteady drag coefficient can be estimated in the same way using the following equation:

$$C_{D_{\tilde{\alpha}^2}}(k)\,\tilde{\alpha}^2 + C_{D_{\tilde{\alpha}\frac{d\tilde{\alpha}}{d\tau}}}(k)\,\tilde{\alpha}\frac{d\tilde{\alpha}}{d\tau} + C_{D_{\frac{d\tilde{\alpha}}{d\tau}^2}}(k)\frac{d\tilde{\alpha}}{d\tau}^2 = \frac{\partial \tilde{C}_D}{\partial \tilde{C}_L}(\bar{s})\left[C_{L_{\tilde{\alpha}}}(k)\,\tilde{\alpha} + C_{L_{\dot{\alpha}}}\frac{d\tilde{\alpha}}{d\tau}\right]^2 \tag{93}$$

III. Determination of Dynamic Stability Derivatives of Transonic Truss-Braced Wing

The dynamic stability derivative estimation method is applied to the TTBW to illustrate the procedure. A series of unsteady RANS CFD simulations of pitch, plunge, roll, yaw, sideslip and axial airspeed oscillations of the Mach 0.8 TTBW is conducted in FUN3D.[4,12] The aircraft CG is the center of the pitch, roll, and yaw oscillations. The FUN3D tetrahedral prism mesh has about 96 million nodes. The Roe's flux-difference splitting scheme and the Spalart-Allmaras turbulence model are used in the simulations. An optimized second-order backward finite-difference scheme is used in the time integration. The oscillations are about the trim points at the design lift coefficient $C_L = 0.695$ and an altitude of 46,716 ft corresponding to the mid-cruise gross weight of 130,486 lbs for the Mach 0.8 TTBW. Figure 3 is an instantaneous surface pressure contour plot of the Mach 0.8 TTBW in pitch oscillations.

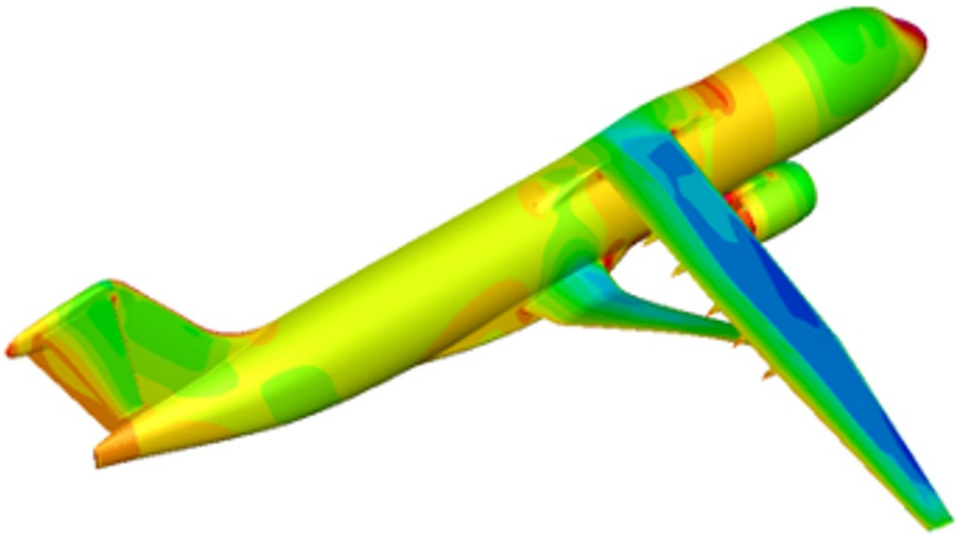

Figure 3. Mach 0.8 Transonic Truss Braced-Wing Instantaneous Pressure Contour In Pitch Oscillations

The frequency data is generated at four reduced frequencies $k = 0.01$, 0.02, 0.1, and 0.2. In addition, steady state data corresponding to $k = 0$ obtained from the steady state stability derivatives computed by steady state RANS simulations are also included. A spline fit is performed to generate the frequency response data over a reduced frequency range from 0.02 to 0.2. A regression is then performed using the second-order transfer function in Eq. (2). In

some cases, A fourth-order transfer function is used to improve accuracy for the pitch rate dynamic stability derivative estimation.

The estimation of the dynamic stability derivatives with respect to the angle of attack and pitch rate has been obtained previously.[4] The estimation of the additional dynamic stability derivatives is presented in this paper.

A. Dynamic Stability Derivatives Due to Angle of Attack

The plots of the unsteady lift and pitching moment versus the angle of attack $\tilde{\alpha}$ for the Mach 0.8 TTBW are shown in Figs. 12(a) and (b), respectively. The analytical results using the Fourier series decomposition are compared to the FUN3D results.

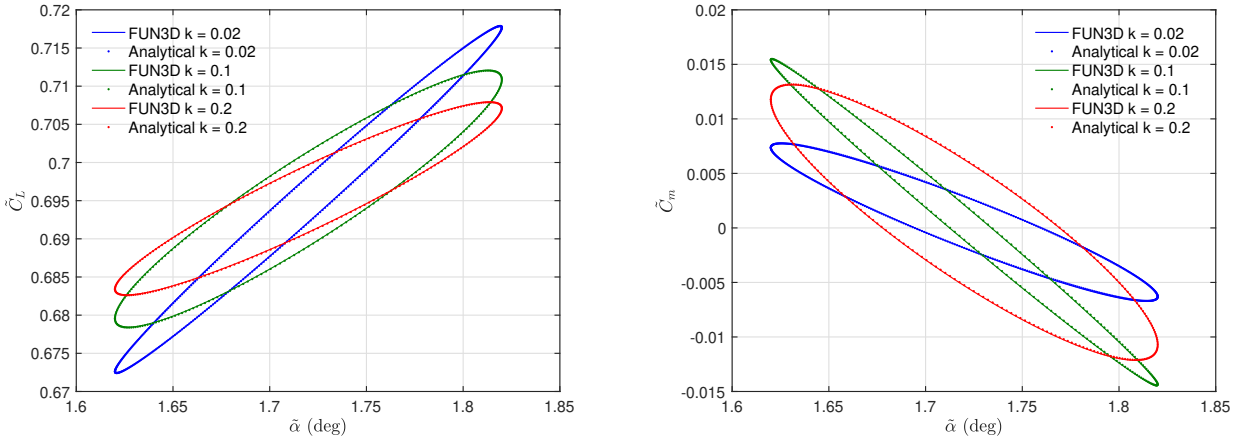

(a) (b)

Figure 4. Mach 0.8 TTBW Unsteady Lift and Pitching Moment Coefficients Due to Angle of Attack Oscillations

The dynamic stability derivatives with respect to the angle of attack of the Mach 0.8 obtained from the regression analysis of the plunge oscillations are obtained as

$$\frac{\partial \tilde{C}_L}{\partial \tilde{\alpha}}(\bar{s}) = \left(1 + \frac{-0.6308\bar{s}^2 - 0.0688\bar{s}}{\bar{s}^2 + 0.1995\bar{s} + 0.0099}\right) 13.1881 + 5.0637\bar{s}$$

$$C_{L_{\tilde{\alpha}}}(\bar{s}) = \left(1 + \frac{-0.6308\bar{s}^2 - 0.0688\bar{s}}{\bar{s}^2 + 0.1995\bar{s} + 0.0099}\right) 13.1881$$

$$C_{L_{\dot{\alpha}}} = 5.0637$$

$$\frac{\partial \tilde{C}_m}{\partial \tilde{\alpha}}(\bar{s}) = \left(1 + \frac{-1.8967\bar{s}^2 + 0.4803\bar{s}}{\bar{s}^2 + 0.3193\bar{s} + 0.0255}\right)(-3.5920) - 8.5490\bar{s}$$

$$C_{m_{\tilde{\alpha}}}(\bar{s}) = \left(1 + \frac{-1.8967\bar{s}^2 + 0.4803\bar{s}}{\bar{s}^2 + 0.3193\bar{s} + 0.0255}\right)(-3.5920)$$

$$C_{m_{\dot{\alpha}}} = -8.5490$$

The plots of the transfer functions $\frac{\partial \tilde{C}_L}{\partial \tilde{\alpha}}(k)$ and $\frac{\partial \tilde{C}_m}{\partial \tilde{\alpha}}(k)$ obtained from the frequency-domain regression are shown in Figs. 5(a)-(b), respectively.

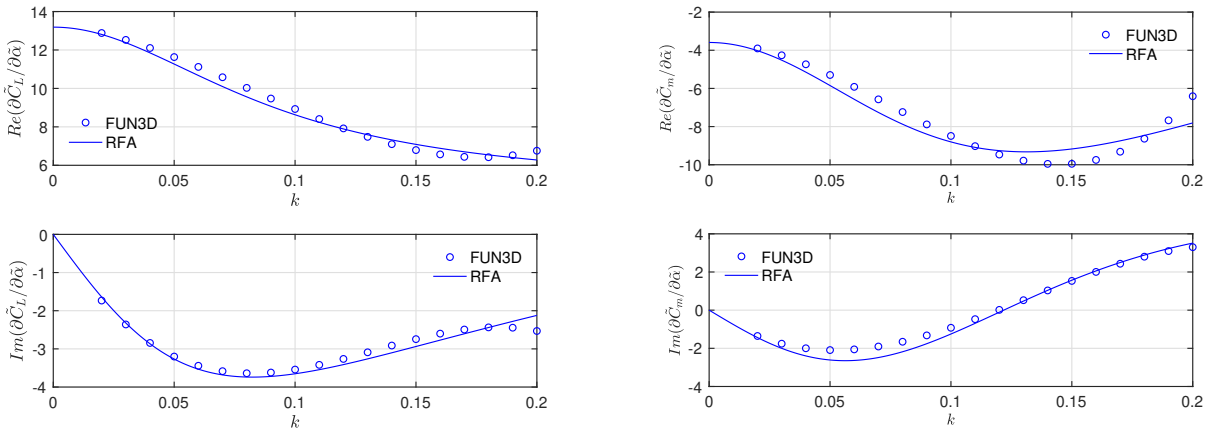

(a) (b)

Figure 5. Mach 0.8 TTBW $\frac{\partial\tilde{C}_L}{\partial\tilde{\alpha}}(k)$ and $\frac{\partial\tilde{C}_m}{\partial\tilde{\alpha}}(k)$ Regression

The unsteady drag coefficient is expressed in the component form as

$$C_D = \bar{C}_D + C_{D_{\tilde{\alpha}}}(k)\,\tilde{\alpha} + C_{D_{\tilde{\alpha}^2}}(k)\,\tilde{\alpha}^2 \tag{94}$$

The linear contribution $C_{D_{\tilde{\alpha}}}\tilde{\alpha}$ is proportional to the unsteady lift coefficient $\tilde{C}_L$, where as the quadratic contribution $C_{D_{\tilde{\alpha}^2}}\tilde{\alpha}^2$ is proportional to $\tilde{C}_L^2$. Figures 6(a)-(b) show the plots of the linear contribution $C_{D_{\tilde{\alpha}}}\tilde{\alpha}$ and quadratic contribution $C_{D_{\tilde{\alpha}^2}}\tilde{\alpha}^2$ versus the unsteady lift coefficient $\tilde{C}_L$, respectively.

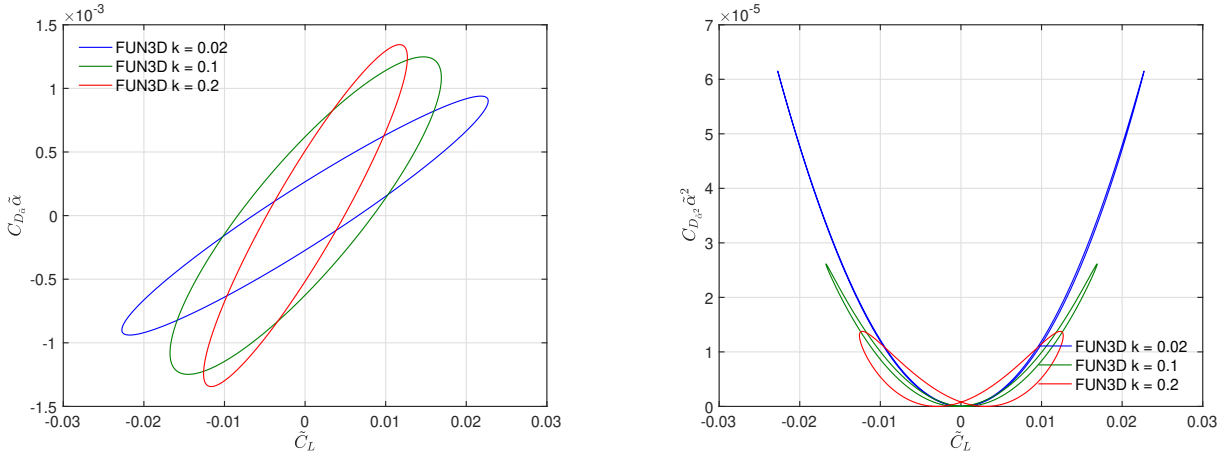

(a) (b)

Figure 6. Mach 0.8 TTBW Linear and Quadratic Unsteady Drag Coefficients $C_{D_{\tilde{\alpha}}}\tilde{\alpha}$ and $C_{D_{\tilde{\alpha}^2}}\tilde{\alpha}^2$ Due to Angle of Attack Oscillations

The transfer functions of the unsteady drag coefficient with respect to the unsteady lift coefficient are obtained by the frequency-domain regression as

$$\frac{\partial\tilde{C}_D}{\partial\tilde{C}_L}(\bar{s}) = \left(1 + \frac{2.03085\bar{s}^2 + 0.53971\bar{s}}{\bar{s}^2 + 0.39908\bar{s} + 0.03982}\right) 0.04004$$

$$\frac{\partial\tilde{C}_D}{\partial\tilde{C}_L^2}(\bar{s}) = \left(1 + \frac{2930.07831\bar{s}^4 - 201.54425\bar{s}^3 + 196.91406\bar{s}^2 - 8.25138\bar{s}}{\bar{s}^4 + 6.94493\bar{s}^3 + 18.06109\bar{s}^2 + 20.84655\bar{s} + 9.01090}\right) 0.11717$$

Figures 7(a)-(b) show the plots of the transfer functions of the unsteady drag coefficient.

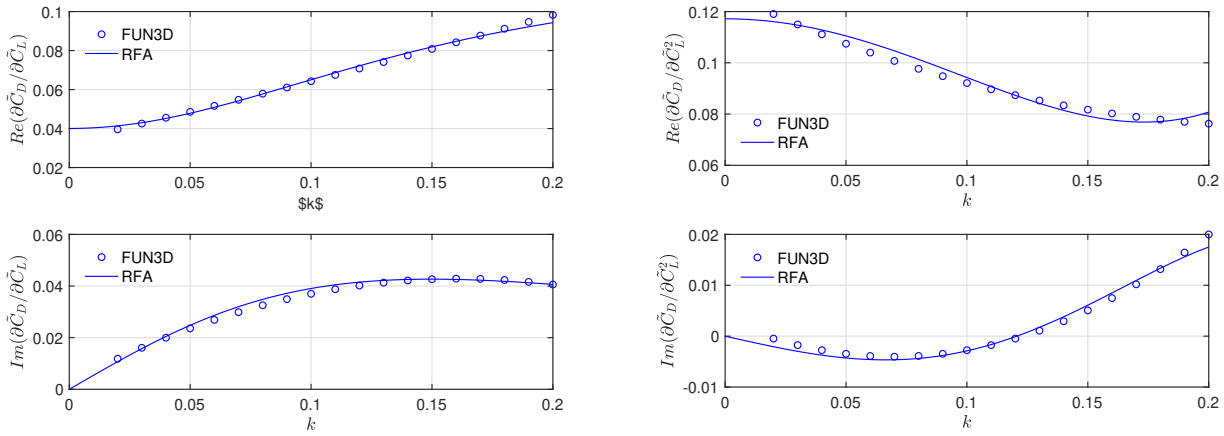

(a) (b)

Figure 7. Mach 0.8 TTBW Transfer Functions of Unsteady Drag Coefficient $\frac{\partial\tilde{C}_D}{\partial\tilde{C}_L}(k)$ and $\frac{\partial\tilde{C}_D}{\partial\tilde{C}_L^2}(k)$

The dynamic stability derivatives of the unsteady drag coefficient are established as

$$C_{D_{\tilde{\alpha}}}(\bar{s}) = \frac{\partial\tilde{C}_D}{\partial\tilde{C}_L}(\bar{s})C_{L_{\tilde{\alpha}}}(\bar{s}) = \left(1+\frac{2.03085\bar{s}^2+0.53971\bar{s}}{\bar{s}^2+0.39908\bar{s}+0.03982}\right)\left(1+\frac{-0.63080\bar{s}^2-0.06881\bar{s}}{\bar{s}^2+0.19950\bar{s}+0.00995}\right)0.52810$$

$$C_{D_{\dot{\alpha}}}(\bar{s}) = \frac{\partial\tilde{C}_D}{\partial\tilde{C}_L}(\bar{s})C_{L_{\dot{\alpha}}} = \left(1+\frac{2.03085\bar{s}^2+0.53971\bar{s}}{\bar{s}^2+0.39908\bar{s}+0.03982}\right)0.20277$$

B. Dynamic Stability Derivatives Due to Pitch Rate

In order to estimate the dynamic stability derivatives with respect to the pitch rate, the contribution of the angle of attack is removed from the unsteady lift and pitching moment coefficients first via Eq. (74) or (78). Figures 8(a)-(b) are the plots of the unsteady lift and pitching moment coefficients versus the nondimensional pitch rate $\tilde{q}$ for the Mach 0.8 TTBW, respectively.

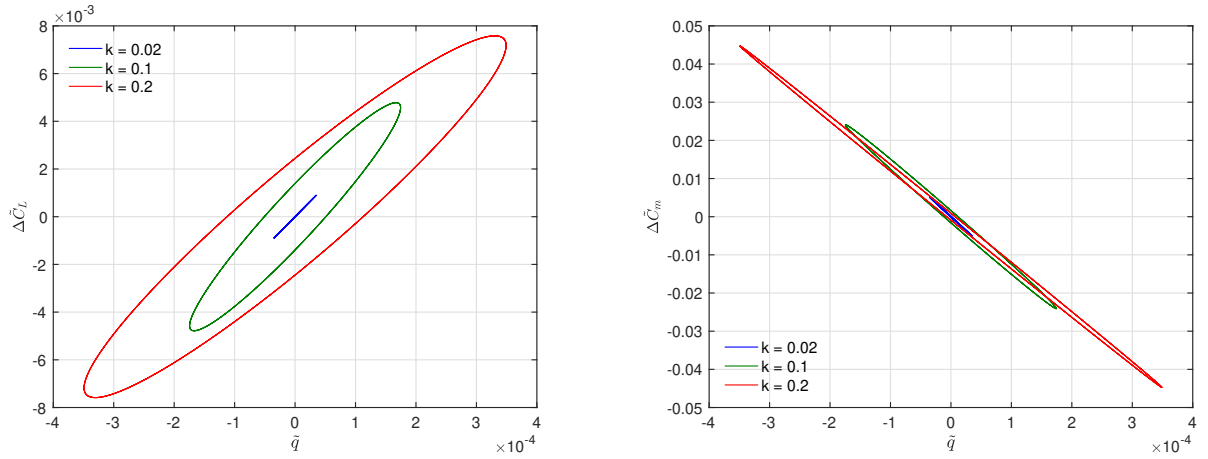

(a) (b)

Figure 8. Mach 0.8 TTBW Unsteady Lift and Pitching Moment Coefficients without Angle of Attack Contribution Due to Pitch Oscillations

The dynamic stability derivatives with respect to the pitch rate of the Mach 0.8 obtained from the regression analysis of the pitch oscillations are obtained as

$$\frac{\partial \Delta \tilde{C}_L}{\partial \tilde{q}}(\bar{s}) = \left(1 + \frac{14.8692\bar{s}^4 + 16.1254\bar{s}^3 + 3.6476\bar{s}^2 + 0.3994\bar{s}}{\bar{s}^4 + 1.5466\bar{s}^3 + 0.8966\bar{s}^2 + 0.2309\bar{s} + 0.0223}\right) 25.0453 - 496.4001\bar{s}$$

$$C_{L_{\tilde{q}}}(\bar{s}) = \left(1 + \frac{14.8692\bar{s}^4 + 16.1254\bar{s}^3 + 3.6476\bar{s}^2 + 0.3994\bar{s}}{\bar{s}^4 + 1.5466\bar{s}^3 + 0.8966\bar{s}^2 + 0.2309\bar{s} + 0.0223}\right) 25.0453$$

$$C_{L_{\dot{q}}} = -496.4001$$

$$\frac{\partial \Delta \tilde{C}_m}{\partial \tilde{q}}(\bar{s}) = \left(1 + \frac{5.7138675\bar{s}^4 + 2.2546\bar{s}^3 + 0.4550\bar{s}^2 + 0.0272\bar{s}}{\bar{s}^4 + 1.1741\bar{s}^3 + 0.5169\bar{s}^2 + 0.1011\bar{s} + 0.0074}\right)(-146.0690) + 714.7804\bar{s}$$

$$C_{m_{\tilde{q}}}(\bar{s}) = \left(1 + \frac{5.7138675\bar{s}^4 + 2.2546\bar{s}^3 + 0.4550\bar{s}^2 + 0.0272\bar{s}}{\bar{s}^4 + 1.1741\bar{s}^3 + 0.5169\bar{s}^2 + 0.1011\bar{s} + 0.0074}\right)(-146.0690)$$

$$C_{m_{\dot{q}}} = 714.7804$$

The plots of the transfer functions $\frac{\partial \Delta \tilde{C}_L}{\partial \tilde{q}}(k)$ and $\frac{\partial \Delta \tilde{C}_m}{\partial \tilde{q}}(k)$ obtained from the frequency-domain regression are shown in Figs. 9(a)-(b), respectively.

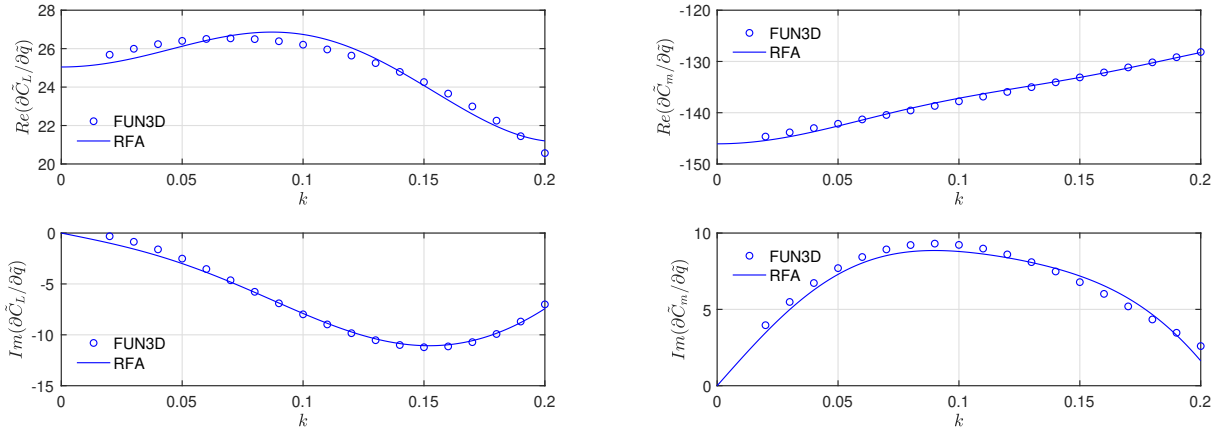

(a) (b)

Figure 9. Mach 0.8 TTBW $\frac{\partial \Delta \tilde{C}_L}{\partial \tilde{q}}(k)$ and $\frac{\partial \Delta \tilde{C}_m}{\partial \tilde{q}}(k)$ Regression

The unsteady drag coefficient is expressed in the component form as

$$C_D = \bar{C}_D + C_{D_{\tilde{\theta}}}\tilde{\theta} + C_{D_{\tilde{\theta}^2}}\tilde{\theta}^2 \tag{95}$$

The plots of the linear contribution $C_{D_{\tilde{\theta}}}\tilde{\theta}$ and quadratic contribution $C_{D_{\tilde{\theta}^2}}\tilde{\theta}^2$ versus the unsteady lift coefficient $\tilde{C}_L$ are shown in Fig. 10(a)-(b), respectively.

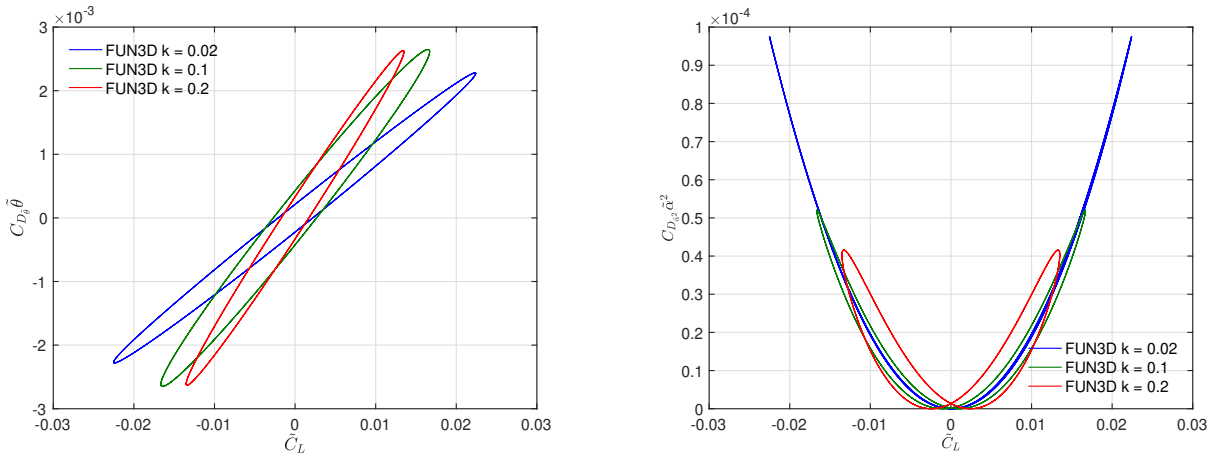

(a) (b)

Figure 10. Mach 0.8 TTBW Linear and Quadratic Unsteady Drag Coefficients $C_{D_{\tilde{\theta}}}\tilde{\theta}$ and $C_{D_{\tilde{\theta}^2}}\tilde{\theta}^2$ Due to Pitch Oscillations

The transfer functions of the unsteady drag coefficient with respect to the unsteady lift coefficient are obtained by the frequency-domain regression as

$$\frac{\partial \tilde{C}_D}{\partial \tilde{C}_L}(\bar{s}) = \left(1 + \frac{-1.1500\bar{s}^2 + 0.5576\bar{s}}{\bar{s}^2 + 0.5630\bar{s} + 0.0668}\right) 0.0907$$

$$\frac{\partial \tilde{C}_D}{\partial \tilde{C}_L^2}(\bar{s}) = \left(1 + \frac{862.7758\bar{s}^4 + 10.5057\bar{s}^3 + 8.7099\bar{s}^2 - 2.5961\bar{s}}{\bar{s}^4 + 5.7730\bar{s}^3 + 12.4761\bar{s}^2 + 11.9616\bar{s} + 4.2926}\right) 0.1910$$

Figures 11 (a)-(b) show the plots of the transfer functions of the unsteady drag coefficient. The transfer function $\frac{\partial \tilde{C}_D}{\partial \tilde{C}_L^2}(k)$ is more difficult to obtained and therefore is less accurate than the transfer function $\frac{\partial \tilde{C}_D}{\partial \tilde{C}_L}(k)$. A 4$^{\text{th}}$-order regression is needed to increase accuracy which still could be further improved with perhaps higher-order regression.

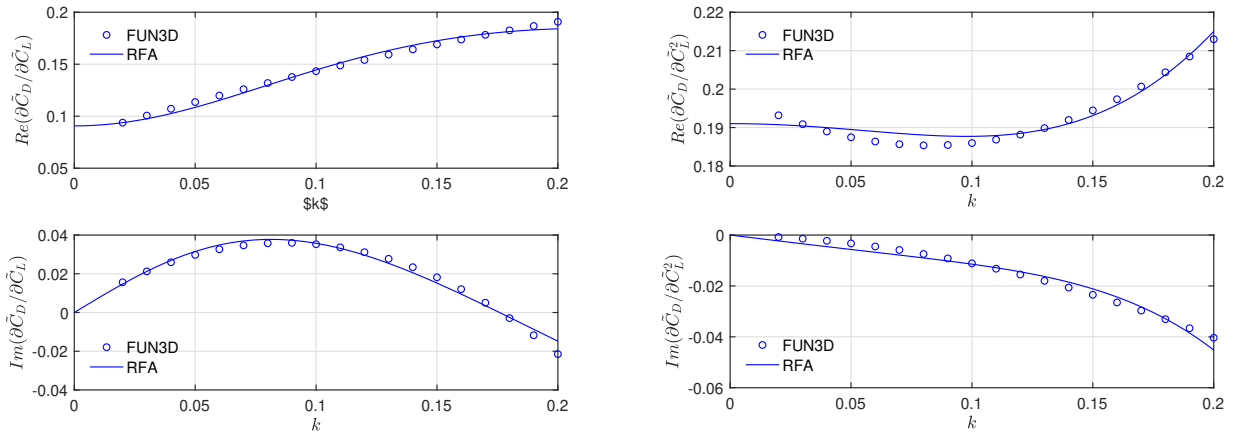

(a) (b)

Figure 11. Mach 0.8 TTBW $\frac{\partial \tilde{C}_D}{\partial \tilde{C}_L}(k)$ and $\frac{\partial \tilde{C}_D}{\partial \tilde{C}_L^2}(k)$ Regression

The dynamic stability derivatives of the unsteady drag coefficient are then established as

$$C_{D_{\tilde{q}}}(\bar{s}) = \frac{\partial \tilde{C}_D}{\partial \tilde{C}_L}(\bar{s}) C_{L_{\tilde{q}}}(\bar{s})$$
$$= \left(1 + \frac{-1.1500\bar{s}^2 + 0.5576\bar{s}}{\bar{s}^2 + 0.5630\bar{s} + 0.0668}\right)\left(1 + \frac{14.8692\bar{s}^4 + 16.1254\bar{s}^3 + 3.6476\bar{s}^2 + 0.3994\bar{s}}{\bar{s}^4 + 1.5466\bar{s}^3 + 0.8966\bar{s}^2 + 0.2309\bar{s} + 0.0223}\right) 2.2714$$

$$C_{D_{\hat{q}}}(\bar{s}) = \frac{\partial \tilde{C}_D}{\partial \tilde{C}_L}(\bar{s}) C_{L_{\hat{q}}} = \left(1 + \frac{-1.1500\bar{s}^2 + 0.5576\bar{s}}{\bar{s}^2 + 0.5630\bar{s} + 0.0668}\right) 3.01233$$

C. Dynamic Stability Derivatives Due to Axial Airspeed

The plots of the unsteady lift and pitching moment versus the nondimensional axial airspeed $\tilde{u}$ for the Mach 0.8 TTBW are shown in Figs. 12(a) and (b), respectively. The analytical results using the Fourier series decomposition are compared to the FUN3D results.

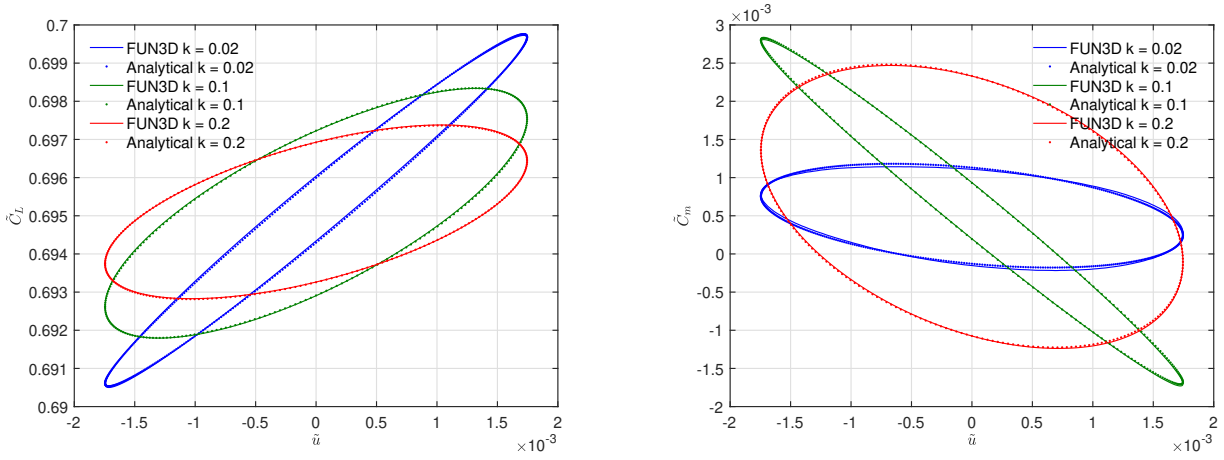

(a) (b)

Figure 12. Mach 0.8 TTBW Unsteady Lift and Pitching Moment Coefficients Due to Axial Airspeed Oscillations

The dynamic stability derivatives with respect to the axial airspeed are obtained as

$$\frac{\partial \tilde{C}_L}{\partial \tilde{u}}(\bar{s}) = \left(1 + \frac{-0.07398\bar{s}^2 - 0.2738\bar{s}}{\bar{s}^2 + 0.3999\bar{s} + 0.03998}\right) 2.5391 - 4.3629\bar{s}$$

$$C_{L_{\tilde{u}}}(\bar{s}) = \left(1 + \frac{-0.07398\bar{s}^2 - 0.2738\bar{s}}{\bar{s}^2 + 0.3999\bar{s} + 0.03998}\right) 2.5391$$

$$C_{L_{\hat{u}}} = -4.3629$$

$$\frac{\partial \tilde{C}_m}{\partial \tilde{u}}(\bar{s}) = \left(1 + \frac{-15.9868\bar{s}^2 + 1.9659\bar{s}}{\bar{s}^2 + 0.2798\bar{s} + 0.01957}\right)(-0.1474) - 2.9338\bar{s}$$

$$C_{m_{\tilde{u}}}(\bar{s}) = \left(1 + \frac{-15.9868\bar{s}^2 + 1.9659\bar{s}}{\bar{s}^2 + 0.2798\bar{s} + 0.01957}\right)(-0.1474)$$

$$C_{m_{\hat{u}}} = -2.9338$$

The plots of the transfer functions $\frac{\partial \tilde{C}_L}{\partial \tilde{u}}(k)$ and $\frac{\partial \tilde{C}_m}{\partial \tilde{u}}(k)$ obtained from the frequency-domain regression are shown in Figs. 13(a)-(b), respectively.

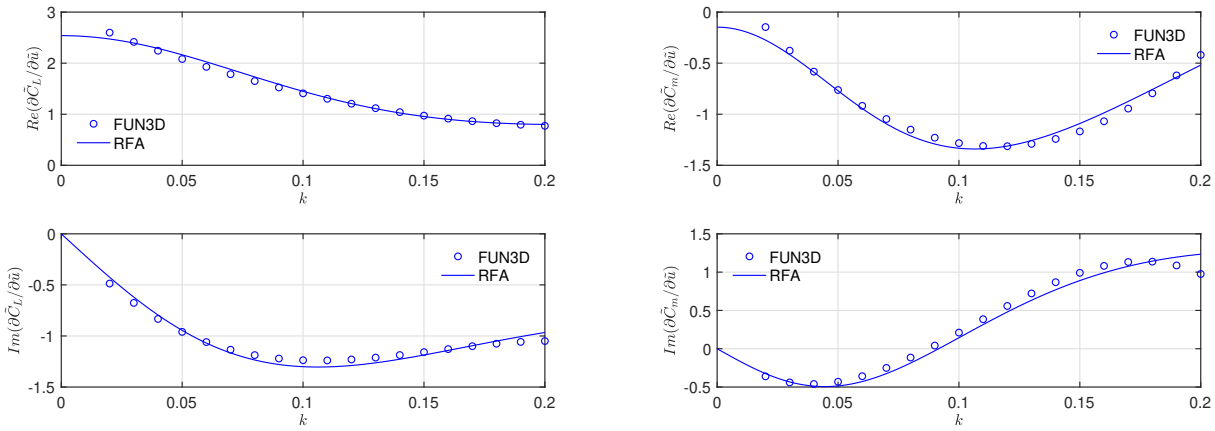

(a) (b)

Figure 13. Mach 0.8 TTBW $\frac{\partial\tilde{C}_L}{\partial\tilde{u}}(k)$ and $\frac{\partial\tilde{C}_m}{\partial\tilde{u}}(k)$ Regression

The unsteady drag coefficient for the axial airspeed oscillations is analyzed. The unsteady drag coefficient is expressed in the component form as

$$C_D = \bar{C}_D + C_{D_{\tilde{u}}}(k)\,\tilde{u} + C_{D_{\tilde{u}^2}}(k)\,\tilde{u}^2 \tag{96}$$

The linear contribution $C_{D_{\tilde{u}}}\tilde{u}$ is proportional to the unsteady lift coefficient $\tilde{C}_L$, where as the quadratic contribution $C_{D^2_{\tilde{u}}}\tilde{u}^2$ is proportional to $\tilde{C}_L^2$. Figures 14(a)-(b) show the plots of the linear contribution $C_{D_{\tilde{\alpha}}}\tilde{\alpha}$ and quadratic contribution $C_{D_{\tilde{\alpha}^2}}\tilde{\alpha}^2$ versus the unsteady lift coefficient $\tilde{C}_L$, respectively.

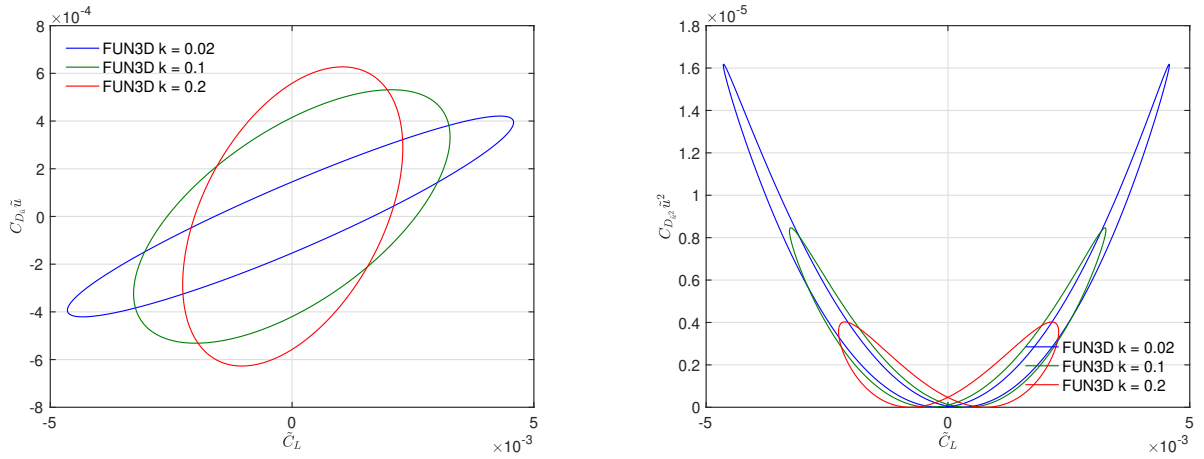

(a) (b)

Figure 14. Mach 0.8 TTBW Linear and Quadratic Unsteady Drag Coefficients $C_{D_{\tilde{u}}}\tilde{u}$ and $C_{D_{\tilde{u}^2}}\tilde{u}^2$ Due to Axial Airspeed Oscillations

The transfer functions of the unsteady drag coefficient with respect to the unsteady lift coefficient due to the axial airspeed oscillations are obtained as

$$\frac{\partial\tilde{C}_D}{\partial\tilde{C}_L}(\bar{s}) = \left(1 + \frac{21.9189\bar{s}^2 + 2.2871\bar{s}}{\bar{s}^2 + 1.6045\bar{s} + 0.1421}\right)\left(1 + \frac{-0.07398\bar{s}^2 - 0.2738\bar{s}}{\bar{s}^2 + 0.3999\bar{s} + 0.03998}\right)0.08455$$

$$\frac{\partial\tilde{C}_D}{\partial\tilde{C}_L^2}(\bar{s}) = \left(1 + \frac{6315.7688\bar{s}^4 + 3346.2550\bar{s}^3 + 189.3076\bar{s}^2 + 65.3783\bar{s}}{\bar{s}^4 + 14.3414\bar{s}^3 + 0.7418\bar{s}^2 + 119.8428\bar{s} + 26.3939}\right)0.7602$$

Figures 15(a)-(b) show the plots of the transfer functions of the unsteady drag coefficient due to the axial airspeed oscillations.

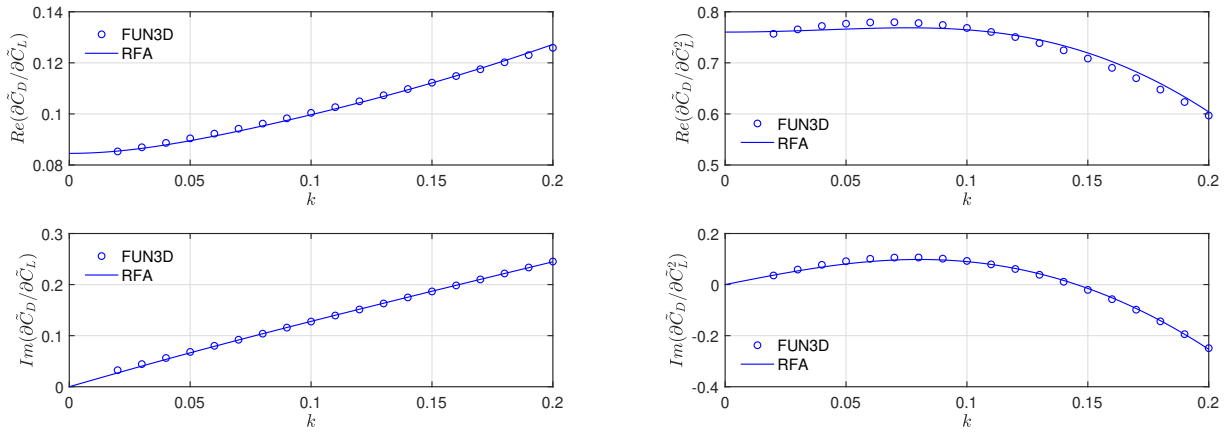

(a) (b)

Figure 15. Mach 0.8 TTBW $\frac{\partial\tilde{C}_D}{\partial\tilde{C}_L}(k)$ and $\frac{\partial\tilde{C}_D}{\partial\tilde{C}_L^2}(k)$ Regression

The dynamic stability derivatives of the unsteady drag coefficient are established as

$$C_{D_{\tilde{u}}}(\bar{s}) = \frac{\partial\tilde{C}_D}{\partial\tilde{C}_L}(\bar{s})\,C_{L_{\tilde{u}}}(\bar{s}) = \left(1+\frac{21.9189\bar{s}^2+2.2871\bar{s}}{\bar{s}^2+1.6045\bar{s}+0.1421}\right)\left(1+\frac{-0.63080\bar{s}^2-0.06881\bar{s}}{\bar{s}^2+0.19950\bar{s}+0.00995}\right)0.2147$$

$$C_{D_{\dot{\tilde{u}}}}(\bar{s}) = \frac{\partial\tilde{C}_D}{\partial\tilde{C}_L}(\bar{s})\,C_{L_{\dot{u}}} = \left(1+\frac{21.9189\bar{s}^2+2.2871\bar{s}}{\bar{s}^2+1.6045\bar{s}+0.1421}\right)(-0.3689)$$

D. Dynamic Stability Derivatives Due to Angle of Sideslip Dynamics

The plots of the unsteady side force, rolling moment, and yawing moment coefficients versus the angle of sideslip $\tilde{\beta}$ for the Mach 0.8 TTBW are shown in Figs. 16(a), (b), and (c), respectively. The analytical results using the Fourier series decomposition are compared to the FUN3D results.

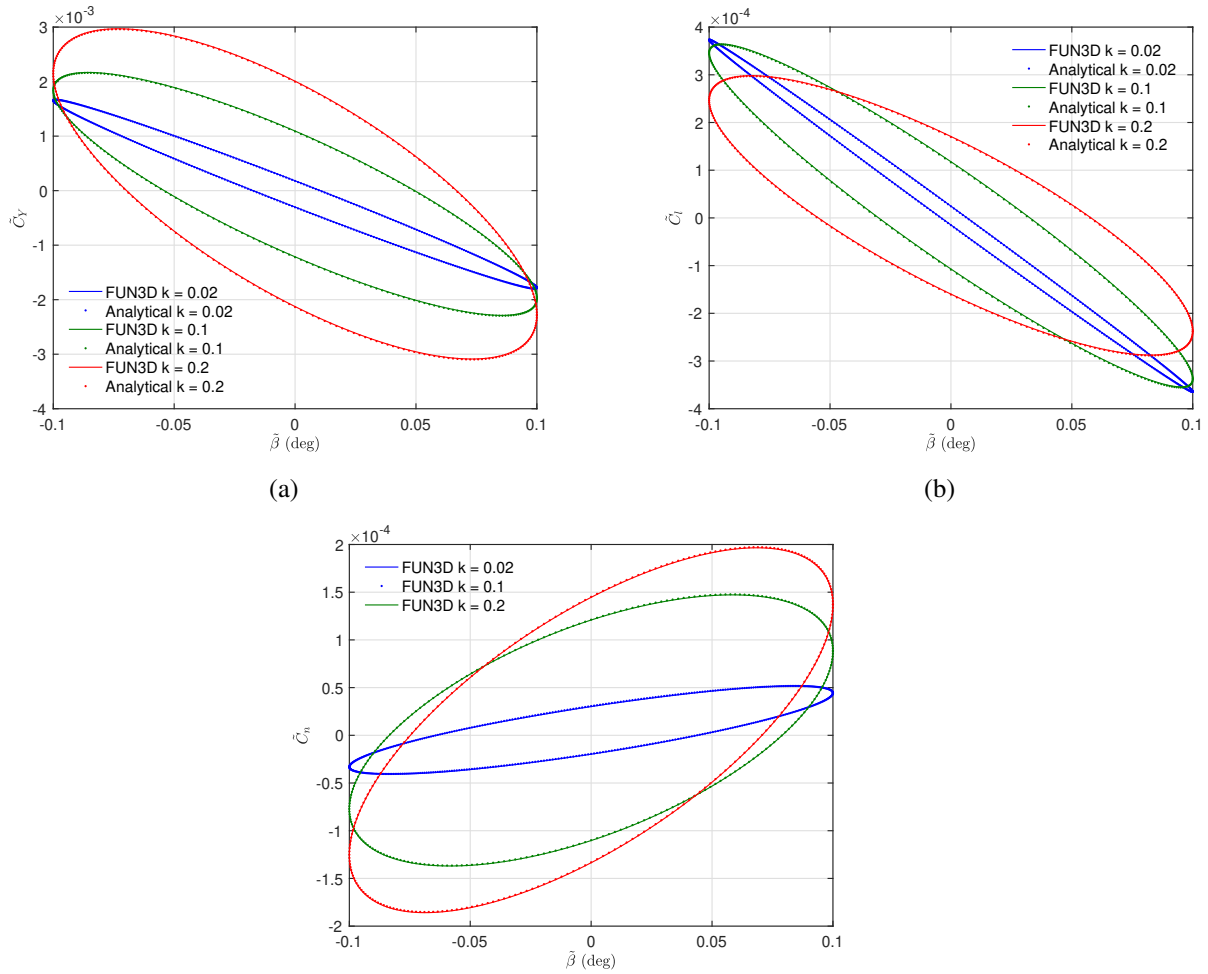

Figure 16. Mach 0.8 TTBW Unsteady Side Force, Rolling Moment, and Pitching Moment Coefficients Due to Angle of Sideslip Oscillations

The dynamic stability derivatives with respect to the angle of sideslip are obtained as

$$\frac{\partial \tilde{C}_Y}{\partial \tilde{\beta}}(\bar{s}) = \left(1 + \frac{58\bar{s}^4 + 694\bar{s}^3 + 3512\bar{s}^2 + 6464\bar{s}}{\bar{s}^4 + 29\bar{s}^3 + 313\bar{s}^2 + 1504\bar{s} + 2712}\right)(-0.9951) + 2.7355\bar{s}$$

$$C_{Y_{\tilde{\beta}}}(\bar{s}) = \left(1 + \frac{58\bar{s}^4 + 694\bar{s}^3 + 3512\bar{s}^2 + 6464\bar{s}}{\bar{s}^4 + 29\bar{s}^3 + 313\bar{s}^2 + 1504\bar{s} + 2712}\right)(-0.9951)$$

$$C_{Y_{\dot{\beta}}} = 2.7355$$

$$\frac{\partial \tilde{C}_l}{\partial \tilde{\beta}}(\bar{s}) = \left(1 + \frac{-5.3420\bar{s}^2 - 17.5890\bar{s}}{\bar{s}^2 + 12.7970\bar{s} + 40.9349}\right)(-0.2078) - 0.1280\bar{s}$$

$$C_{l_{\tilde{\beta}}}(\bar{s}) = \left(1 + \frac{-5.3420\bar{s}^2 - 17.5890\bar{s}}{\bar{s}^2 + 12.7970\bar{s} + 40.9349}\right)(-0.2078)$$

$$C_{l_{\dot{\beta}}} = -0.1280$$

$$\frac{\partial \tilde{C}_n}{\partial \tilde{\beta}}(\bar{s}) = \left(1 + \frac{1238\bar{s}^4 + 14055\bar{s}^3 + 70766\bar{s}^2 + 128513\bar{s}}{\bar{s}^4 + 29\bar{s}^3 + 313\bar{s}^2 + 1507\bar{s} + 2719}\right)0.02316 - 1.1372\bar{s}$$

$$C_{n_{\tilde{\beta}}}(\bar{s}) = \left(1 + \frac{1238\bar{s}^4 + 14055\bar{s}^3 + 70766\bar{s}^2 + 128513\bar{s}}{\bar{s}^4 + 29\bar{s}^3 + 313\bar{s}^2 + 1507\bar{s} + 2719}\right) 0.02316$$

$$C_{n_{\tilde{\beta}}} = -1.1372$$

The plots of the transfer functions $\frac{\partial \tilde{C}_Y}{\partial \tilde{\beta}}(k)$, $\frac{\partial \tilde{C}_l}{\partial \tilde{\beta}}(k)$, and $\frac{\partial \tilde{C}_n}{\partial \tilde{\beta}}(k)$ obtained from the frequency-domain regression are shown in Figs. 17(a), (b), and (c), respectively.

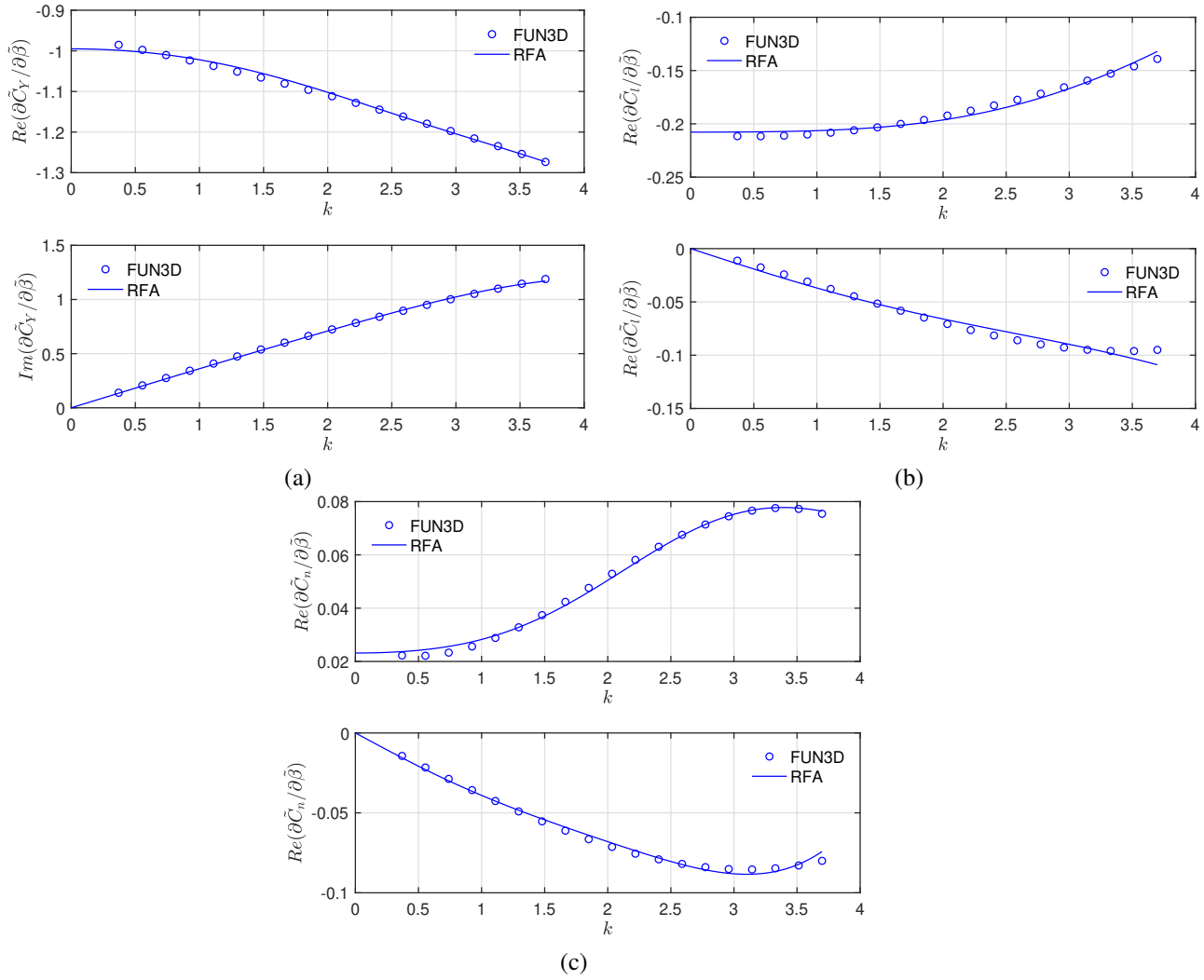

Figure 17. Mach 0.8 TTBW $\frac{\partial \tilde{C}_Y}{\partial \tilde{\beta}}(k)$, $\frac{\partial \tilde{C}_l}{\partial \tilde{\beta}}(k)$ and $\frac{\partial \tilde{C}_n}{\partial \tilde{\beta}}(k)$ Regression

E. Dynamic Stability Derivatives Due to Yaw Rate Dynamics

The contribution of the angle of sideslip to the yaw rate dynamics is removed from the unsteady side force, rolling moment, and yawing moment coefficients. The resulting coefficients then are only dependent on the yaw rate. The plots of the components of the unsteady side force, rolling moment, and yawing moment coefficients versus the nondimensional yaw rate $\tilde{r}$ for the Mach 0.8 TTBW are shown in Figs. 20(a), (b), and (c), respectively.

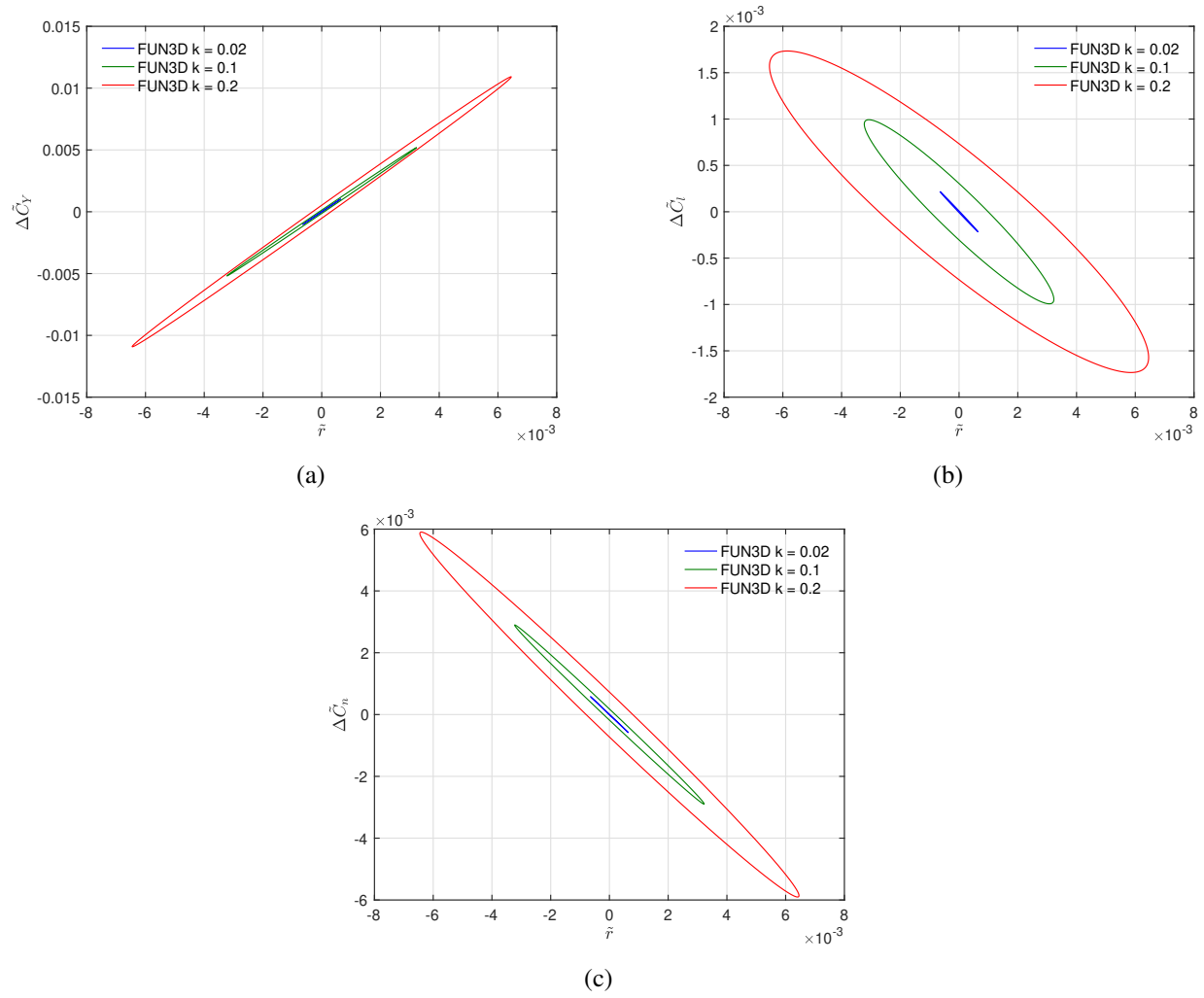

Figure 18. Mach 0.8 TTBW Unsteady Side Force, Rolling Moment, and Yawing Moment Coefficients Due to Yaw Oscillations

The dynamic stability derivatives with respect to the angle of sideslip are obtained as

$$\frac{\partial \tilde{C}_Y}{\partial \tilde{r}}(\bar{s}) = \left(1 + \frac{117922\bar{s}^2 + 10887031\bar{s}}{\bar{s}^2 + 369\bar{s} + 34096}\right) 1.6025 - 512\bar{s}$$

$$C_{Y_{\tilde{r}}}(\bar{s}) = \left(1 + \frac{117922\bar{s}^2 + 10887031\bar{s}}{\bar{s}^2 + 369\bar{s} + 34096}\right) 1.6025$$

$$C_{Y_{\dot{r}}} = -512$$

$$\frac{\partial \tilde{C}_l}{\partial \tilde{r}}(\bar{s}) = \left(1 + \frac{-75\bar{s}^4 - 862\bar{s}^3 - 4282\bar{s}^2 - 7.691\bar{s}}{\bar{s}^4 + 28\bar{s}^3 + 302\bar{s}^2 + 1431\bar{s} + 2540}\right)(-0.3276) - 0.9453\bar{s}$$

$$C_{l_{\tilde{r}}}(\bar{s}) = \left(1 + \frac{-75\bar{s}^4 - 862\bar{s}^3 - 4282\bar{s}^2 - 7.691\bar{s}}{\bar{s}^4 + 28\bar{s}^3 + 302\bar{s}^2 + 1431\bar{s} + 2540}\right)(-0.3276)$$

$$C_{l_{\dot{r}}} = -0.9453$$

$$\frac{\partial \tilde{C}_n}{\partial \tilde{r}}(\bar{s}) = \left(1 + \frac{-129321\bar{s}^2 - 11950374\bar{s}}{\bar{s}^2 + 370\bar{s} + 34163}\right)(-0.8992) - 315\bar{s}$$

$$C_{n_{\tilde{r}}}(\bar{s}) = \left(1 + \frac{-129321\bar{s}^2 - 11950374\bar{s}}{\bar{s}^2 + 370\bar{s} + 34163}\right)(-0.8992)$$

$$C_{n_{\dot{r}}} = -315$$

The plots of the transfer functions $\frac{\partial \tilde{C}_Y}{\partial \tilde{r}}(k)$, $\frac{\partial \tilde{C}_l}{\partial \tilde{r}}(k)$, and $\frac{\partial \tilde{C}_n}{\partial \tilde{r}}(k)$ obtained from the frequency-domain regression are shown in Figs. 19(a), (b), and (c), respectively. The regression is somewhat inaccurate for the side force and yawing moment dynamic stability derivatives.

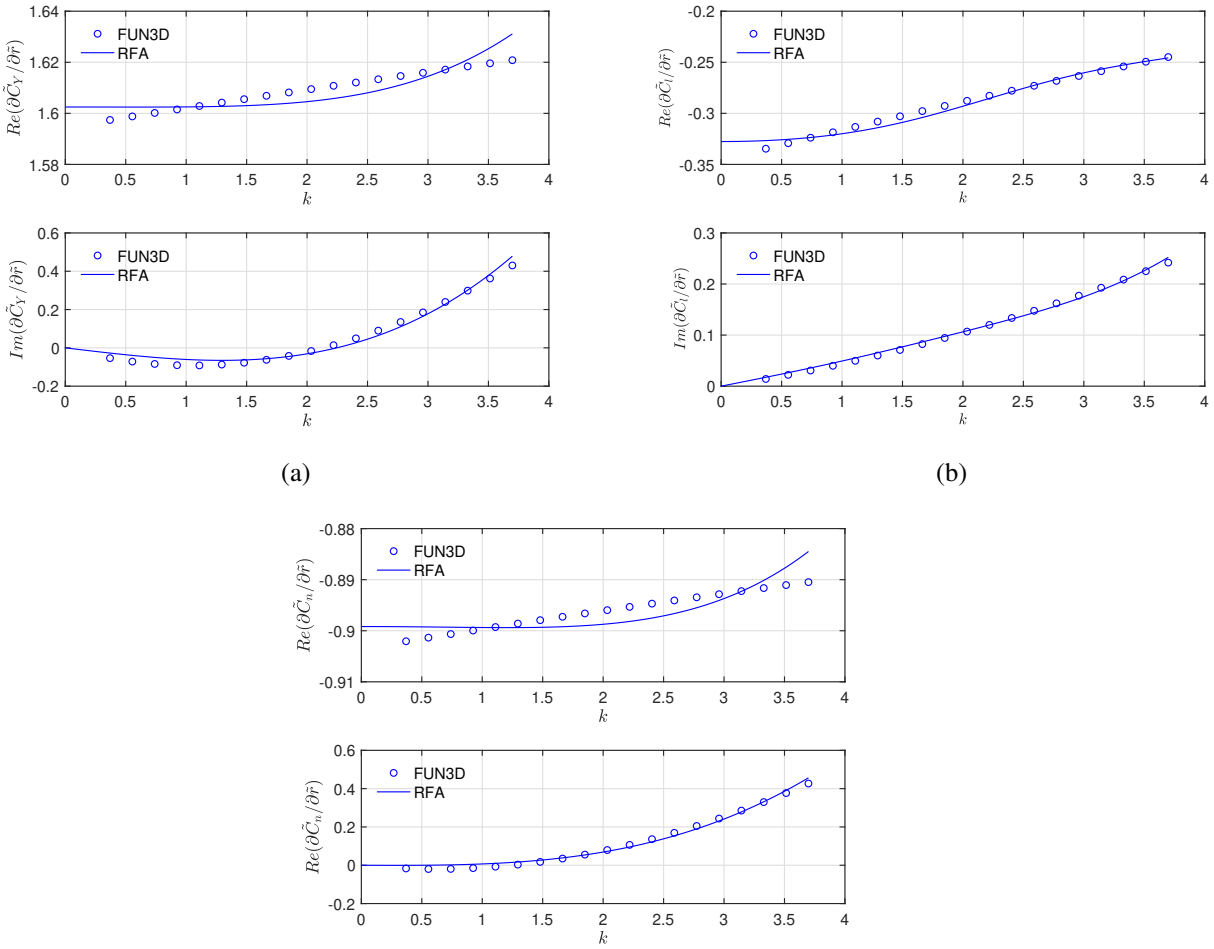

(a) (b)

(c)

Figure 19. Mach 0.8 TTBW $\frac{\partial \tilde{C}_Y}{\partial \tilde{r}}(k)$, $\frac{\partial \tilde{C}_l}{\partial \tilde{r}}(k)$ and $\frac{\partial \tilde{C}_n}{\partial \tilde{r}}(k)$ Regression

F. Dynamic Stability Derivatives Due to Roll Rate Dynamics

The plots of the unsteady side force, rolling moment, and yawing moment coefficients versus the nondimensional roll rate $\tilde{p}$ for the Mach 0.8 TTBW are shown in Figs. 20(a), (b), and (c), respectively. The analytical results using the Fourier series decomposition are compared to the FUN3D results.

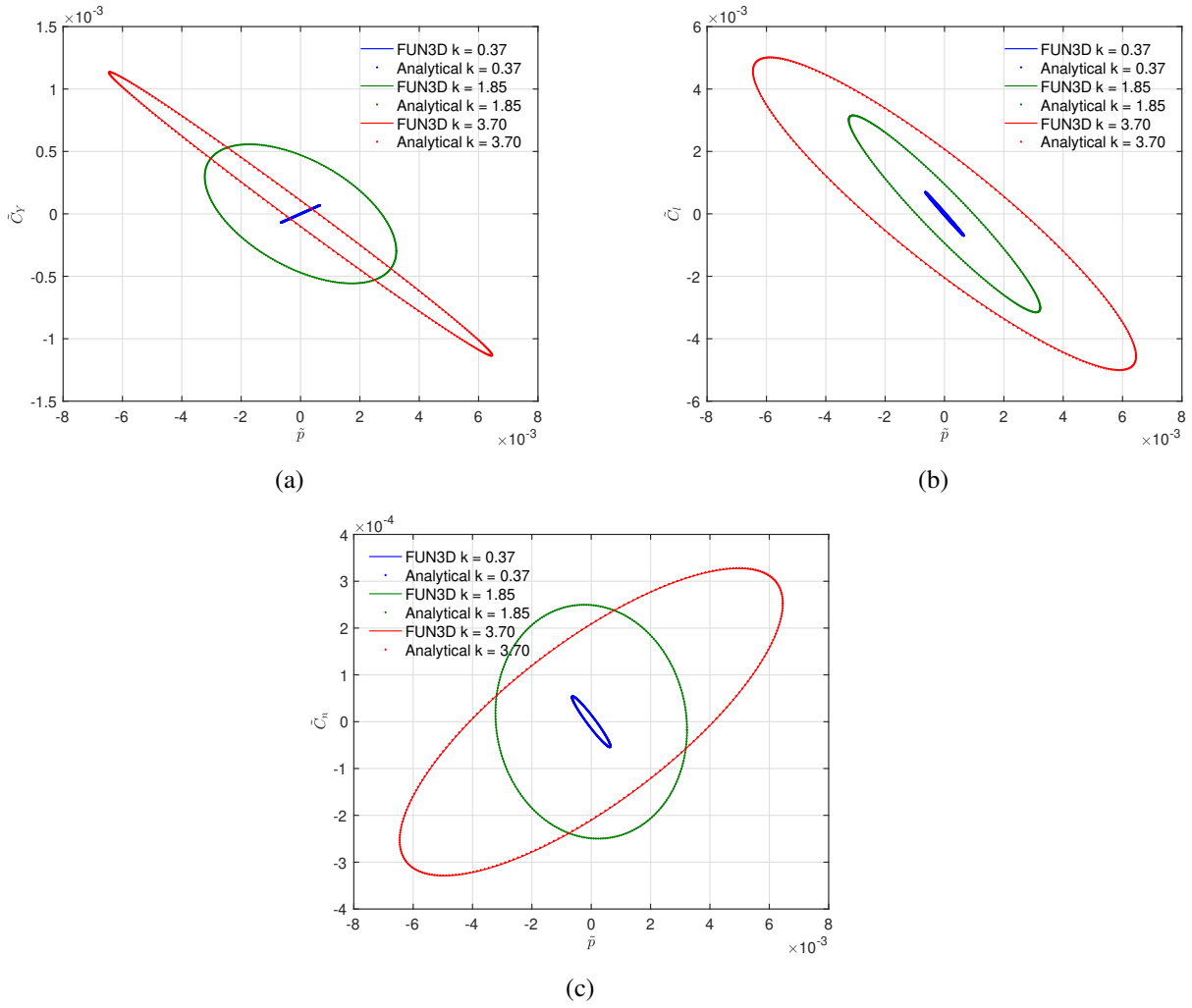

Figure 20. Mach 0.8 TTBW Unsteady Side Force, Rolling Moment, and Yawing Moment Coefficients Due to Roll Oscillations

The dynamic stability derivatives with respect to the roll rate are obtained as

$$\frac{\partial \tilde{C}_Y}{\partial \tilde{p}}(\bar{s}) = \left(1 + \frac{-40978\bar{s}^4 - 876045\bar{s}^3 - 8401608\bar{s}^2 - 29968532\bar{s}}{\bar{s}^4 + 57\bar{s}^3 + 1219\bar{s}^2 + 11576\bar{s} + 41200}\right) 0.07110 - 51.6592\bar{s}$$

$$C_{Y_{\tilde{p}}}(\bar{s}) = \left(1 + \frac{-40978\bar{s}^4 - 876045\bar{s}^3 - 8401608\bar{s}^2 - 29968532\bar{s}}{\bar{s}^4 + 57\bar{s}^3 + 1219\bar{s}^2 + 11576\bar{s} + 41200}\right) 0.07110$$

$$C_{Y_{\dot{p}}} = -51.6592$$

$$\frac{\partial \tilde{C}_l}{\partial \tilde{p}}(\bar{s}) = \left(1 + \frac{-0.5566\bar{s}^2 - 2.4817\bar{s}}{\bar{s}^2 + 7.3939\bar{s} + 13.6675}\right)(-1.0903) + 0.007633\bar{s}$$

$$C_{l_{\tilde{p}}}(\bar{s}) = \left(1 + \frac{-0.5566\bar{s}^2 - 2.4817\bar{s}}{\bar{s}^2 + 7.3939\bar{s} + 13.6675}\right)(-1.0903)$$

$$C_{l_{\dot{p}}} = 0.007633$$

$$\frac{\partial \tilde{C}_n}{\partial \tilde{p}}(\bar{s}) = \left(1 + \frac{20.5282\bar{s}^2 + 20.1665\bar{s}}{\bar{s}^2 + 14.0482\bar{s} + 49.3381}\right)(-0.07114) + 0.09264\bar{s}$$

$$C_{n_{\tilde{p}}}(\bar{s}) = \left(1 + \frac{20.5282\bar{s}^2 + 20.1665\bar{s}}{\bar{s}^2 + 14.0482\bar{s} + 49.3381}\right)(-0.07114)$$

$$C_{n_{\tilde{p}}} = 0.09264$$

The plots of the transfer functions $\frac{\partial \tilde{C}_Y}{\partial \tilde{p}}(k)$, $\frac{\partial \tilde{C}_l}{\partial \tilde{p}}(k)$, and $\frac{\partial \tilde{C}_n}{\partial \tilde{p}}(k)$ obtained from the frequency-domain regression are shown in Figs. 21(a), (b), and (c), respectively.

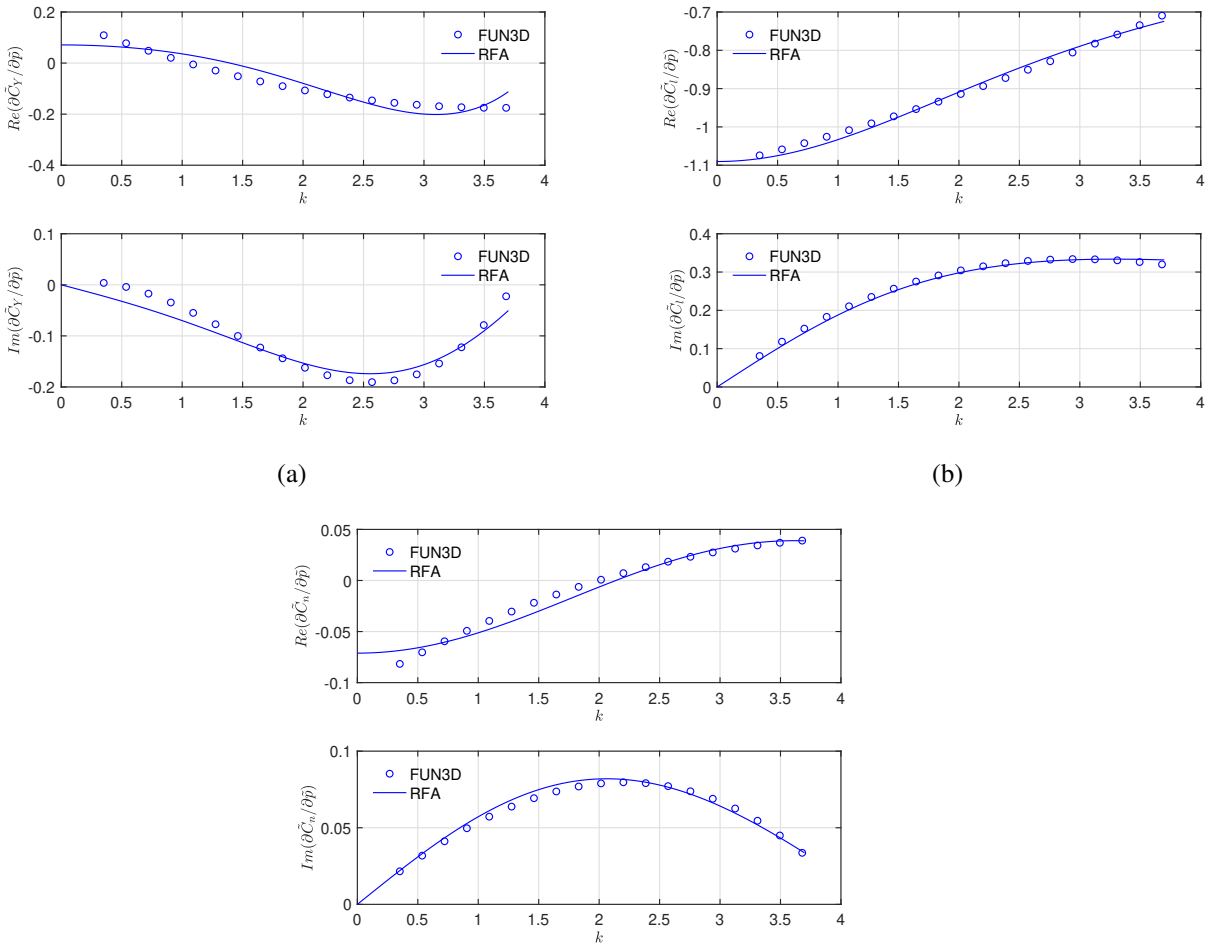

(a) (b)

(c)

Figure 21. Mach 0.8 TTBW $\frac{\partial \tilde{C}_Y}{\partial \tilde{p}}(k)$, $\frac{\partial \tilde{C}_l}{\partial \tilde{p}}(k)$ and $\frac{\partial \tilde{C}_n}{\partial \tilde{p}}(k)$ Regression

IV. Flight Dynamic Analysis of Transonic Truss-Braced Wing

To conduct the flight dynamic stability analysis of the Mach 0.8 TTBW, we obtain the linearized equations of motion of the aircraft in the stability axes about the trim flight condition at Mach 0.8, the altitude of 46,716, and the trim angle of attack $\bar{\alpha} = 1.78^\circ$ corresponding to the design C_L of 0.695.

A. Longitudinal Flight Dynamic Analysis

The equations of motion for longitudinal flight dynamics are given by

$$\dot{h} = V \sin\gamma \tag{97}$$

$$m\dot{V} = -C_D q_\infty S + T\cos\alpha - mg\sin\gamma \tag{98}$$

$$mV\dot{\alpha} = -C_L q_\infty S - T\sin\alpha + mg\cos\gamma + mVq \tag{99}$$

$$I_{yy}\dot{q} = C_m q_\infty S\bar{c} + Tz_e \tag{100}$$

$$\dot{\theta} = q \tag{101}$$

The trim equations for the level flight condition with the flight path angle $\bar{\gamma} = \bar{\theta} - \bar{\alpha} = 0$ are

$$\bar{T}\cos\bar{\alpha} = \bar{C}_D q_\infty S \tag{102}$$

$$\bar{T}\sin\bar{\alpha} = -\bar{C}_L q_\infty S + mg \tag{103}$$

The linearized equations of motion expressed in terms of nondimensional variables are

$$\dot{\tilde{h}} = \frac{2V_\infty}{\bar{c}}\frac{d\tilde{h}}{d\tau} = \frac{V_\infty}{\bar{h}}\left(\tilde{\theta} - \tilde{\alpha}\right) \tag{104}$$

$$mV_\infty\dot{\tilde{u}} = \frac{2mV_\infty^2}{\bar{c}}\frac{d\tilde{u}}{d\tau} = -C_D q_\infty S + \bar{C}_L q_\infty S\tilde{\alpha} - mg\tilde{\theta} \tag{105}$$

$$mV_\infty\dot{\tilde{\alpha}} = \frac{2mV_\infty^2}{\bar{c}}\frac{d\tilde{\alpha}}{d\tau} = -C_L q_\infty S - \bar{C}_D q_\infty S\tilde{\alpha} + \frac{2mV_\infty^2}{\bar{c}}\tilde{q} \tag{106}$$

$$I_{yy}\dot{q} = \frac{4I_{yy}V_\infty^2}{\bar{c}^2}\frac{d\tilde{q}}{d\tau} = C_m q_\infty S\bar{c} \tag{107}$$

$$\frac{d\tilde{\theta}}{d\tau} = \tilde{q} \tag{108}$$

where $\tilde{h} = \dfrac{\Delta h}{\bar{h}}$ and $\tilde{V} = \dfrac{\Delta V}{V_\infty} \approx \tilde{u}$.

The aerodynamic coefficients for longitudinal flight dynamics expressed as functions of the reduced frequency are

$$C_L(\bar{s}) = C_{L_h}\tilde{h} + \left[2\bar{C}_L + C_{L_{\tilde{u}}}(\bar{s}) + C_{L_{\dot{u}}}\bar{s}\right]\tilde{u} + \left[C_{L_{\tilde{\alpha}}}(\bar{s}) + C_{L_{\dot{\alpha}}}\bar{s}\right]\tilde{\alpha} + \left[C_{L_{\tilde{q}}}(\bar{s}) + C_{L_{\dot{q}}}\bar{s}\right]\tilde{q} \tag{109}$$

$$C_D(\bar{s}) = C_{D_h}\tilde{h} + \left[2\bar{C}_D + C_{D_{\tilde{u}}}(\bar{s}) + C_{D_{\dot{u}}}(\bar{s})\,\bar{s}\right]\tilde{u} + \left[C_{D_{\tilde{\alpha}}}(\bar{s}) + C_{D_{\dot{\alpha}}}(\bar{s})\,\bar{s}\right]\tilde{\alpha} + \left[C_{D_{\tilde{q}}}(\bar{s}) + C_{D_{\dot{q}}}(\bar{s})\,\bar{s}\right]\tilde{q} \tag{110}$$

$$C_m(\bar{s}) = \left[C_{m_{\tilde{u}}}(\bar{s}) + C_{m_{\dot{u}}}\bar{s}\right]\tilde{u} + \left[C_{m_{\tilde{\alpha}}}(\bar{s}) + C_{m_{\dot{\alpha}}}\bar{s}\right]\tilde{\alpha} + \left[C_{m_{\tilde{q}}}(\bar{s}) + C_{m_{\dot{q}}}\bar{s}\right]\tilde{q} \tag{111}$$

The stability derivatives with respect to the altitude $\tilde{h}$ are due to the change in the density which can be evaluated analytically.

The linearized equations of motion are then expressed in the nondimensional matrix form as

$$\mathbf{M}_{lon}(\bar{s})\,\bar{s}\mathbf{x}_{lon} = \mathbf{S}_{lon}(\bar{s})\,\mathbf{x}_{lon} \tag{112}$$

where $\mathbf{x}_{lon} = \begin{bmatrix} \tilde{h} & \tilde{u} & \tilde{\alpha} & \tilde{q} & \tilde{\theta} \end{bmatrix}^\top$ is the nondimensional longitudinal aircraft state vector and the nondimensional reduced-frequency dependent matrices $\mathbf{M}_{lon}(\bar{s})$ and $\mathbf{S}_{lon}(\bar{s})$ are given by

$$\mathbf{M}_{lon}(\bar{s}) = \begin{bmatrix} \dfrac{2\bar{h}}{\bar{c}} & 0 & 0 & 0 & 0 \\ 0 & \dfrac{2mV_\infty^2}{q_\infty S\bar{c}} + C_{D_{\dot{u}}}(\bar{s}) & C_{D_{\dot{\alpha}}}(\bar{s}) & C_{D_{\dot{q}}}(\bar{s}) & 0 \\ 0 & C_{L_{\dot{u}}} & \dfrac{2mV_\infty^2}{q_\infty S\bar{c}} + C_{L_{\dot{\alpha}}} & C_{L_{\dot{q}}} & 0 \\ 0 & -C_{m_{\dot{u}}} & -C_{m_{\dot{\alpha}}} & \dfrac{4I_{yy}V_\infty^2}{q_\infty S\bar{c}^3} - C_{m_{\dot{q}}} & 0 \\ 0 & 0 & 0 & 0 & 1 \end{bmatrix} \tag{113}$$

$$\mathbf{S}_{lon}(\bar{s}) = \begin{bmatrix} 0 & 0 & -1 & 0 & 1 \\ -C_{D_h} & -2\bar{C}_D - C_{D_{\tilde{u}}}(\bar{s}) & \bar{C}_L - C_{D_{\tilde{\alpha}}}(\bar{s}) & -C_{D_{\tilde{q}}}(\bar{s}) & -\dfrac{mg}{q_\infty S} \\ -C_{L_h} & -2\bar{C}_L - C_{L_{\tilde{u}}}(\bar{s}) & -\bar{C}_D - C_{L_{\tilde{\alpha}}}(\bar{s}) & \dfrac{2mV_\infty^2}{q_\infty S\bar{c}} - C_{L_{\tilde{q}}}(\bar{s}) & 0 \\ 0 & C_{m_{\tilde{u}}}(\bar{s}) & C_{m_{\tilde{\alpha}}}(\bar{s}) & C_{m_{\tilde{q}}}(\bar{s}) & 0 \\ 0 & 0 & 0 & 1 & 0 \end{bmatrix} \tag{114}$$

The eigenvalues of the longitudinal flight dynamics can be computed as the zeros of the following transfer function matrix which are the roots of the characteristic equation

$$|\mathbf{M}_{lon}(\bar{s})\,\bar{s} - \mathbf{S}_{lon}(\bar{s})| = 0 \tag{115}$$

Figure 22 is the plot of the eigenvalues of the longitudinal flight dynamics of the Mach 0.8 TTBW. All the eigenvalues are stable. For comparison, the eigenvalues of the the longitudinal flight dynamics of the Mach 0.8 TTBW using the steady state stability derivatives by letting $\bar{s} = 0$ in all the dynamic stability derivatives are also computed and plotted. The frequencies and damping of the longitudinal flight dynamic modes are listed in Table 1. The short period mode has higher frequency and damping with the dynamic stability derivatives than with the steady state stability derivatives.

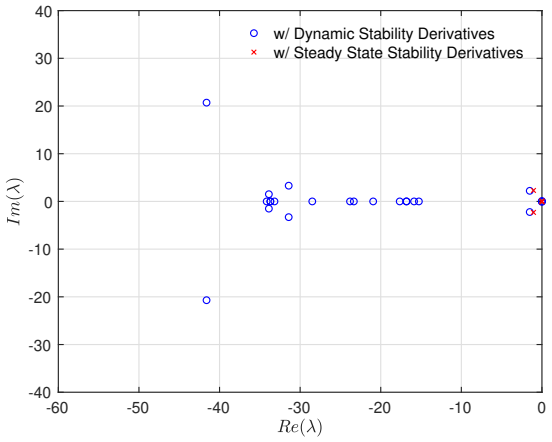

Figure 22. Eigenvalues of Longitudinal Flight Dynamics of Mach 0.8 TTBW

Mode	λ	ω (rad/sec)	ζ
Short Period	$-1.5123 \pm i2.2227$	2.6884	0.5625
Phugoid	$-0.006208 \pm i0.09149$	0.091703	0.06769
Plunge	-0.0008845	0.0008845	1

(a) with Dynamic Stability Derivatives

Mode	λ	ω (rad/sec)	ζ
Short Period	$-1.0509 \pm i2.3033$	2.5317	0.4151
Phugoid	$-0.006543 \pm i0.09147$	0.09171	0.07134
Plunge	-0.0008847	0.0008847	1

(b) with Steady State Stability Derivatives

Table 1. Longitudinal Flight Dynamic Modes

B. Lateral-Directional Flight Dynamic Analysis

The equations of motion for lateral-directional flight dynamics are given by

$$\begin{aligned} mV\dot{\beta} = &\left(C_Y\cos\beta + C_D\sin\beta\right)q_\infty S - T\cos\alpha\sin\beta + mV\left(p\sin\alpha - r\cos\alpha\right) \\ &+ mg\left(\cos\theta\sin\phi\cos\beta + \sin\theta\cos\alpha\sin\beta - \cos\theta\cos\phi\sin\alpha\sin\beta\right) \end{aligned} \tag{116}$$

$$I_{xx}\dot{p} - I_{xz}\dot{r} - I_{xz}pq + \left(I_{zz} - I_{yy}\right)qr = C_l q_\infty Sb \tag{117}$$

$$-I_{xz}\dot{p} + I_{zz}\dot{r} + I_{xz}qr + \left(I_{yy} - I_{xx}\right)pq = C_n q_\infty Sb \tag{118}$$

$$\dot{\phi} = p + q\sin\phi\tan\theta + r\cos\phi\tan\theta \tag{119}$$

The linearized equations of motion expressed in terms of nondimensional variables are

$$mV_\infty\dot{\tilde{\beta}} = \frac{2mV_\infty^2}{b}\frac{d\tilde{\beta}}{d\tau} = C_Y q_\infty S + \frac{2mV_\infty^2}{b}\left(\bar{\alpha}\tilde{p} - \tilde{r}\right) + mg\tilde{\phi} \tag{120}$$

$$I_{xx}\dot{p} - I_{xz}\dot{r} = \frac{4I_{xx}V_\infty^2}{b^2}\frac{d\tilde{p}}{d\tau} - \frac{4I_{xz}V_\infty^2}{b^2}\frac{d\tilde{r}}{d\tau} = C_l q_\infty Sb \tag{121}$$

$$-I_{xz}\dot{p} + I_{zz}\dot{r} = -\frac{4I_{xz}V_\infty^2}{b^2}\frac{d\tilde{p}}{d\tau} + \frac{4I_{zz}V_\infty^2}{b^2}\frac{d\tilde{r}}{d\tau} = C_n q_\infty Sb \tag{122}$$

$$\frac{d\tilde{\phi}}{d\tau} = \tilde{p} + \bar{\theta}\tilde{r} \tag{123}$$

The aerodynamic coefficients for lateral-directional flight dynamics expressed as functions of the reduced frequency are

$$C_Y(\bar{s}) = \left[C_{Y_{\tilde{\beta}}}(\bar{s}) + C_{Y_{\dot{\beta}}}\bar{s}\right]\tilde{\beta} + \left[C_{Y_{\tilde{p}}}(\bar{s}) + C_{Y_{\dot{p}}}\bar{s}\right]\tilde{p} + \left[C_{Y_{\tilde{r}}}(\bar{s}) + C_{Y_{\dot{r}}}\bar{s}\right]\tilde{r} \tag{124}$$

$$C_l(\bar{s}) = \left[C_{l_{\tilde{\beta}}}(\bar{s}) + C_{l_{\dot{\beta}}}\bar{s}\right]\tilde{\beta} + \left[C_{l_{\tilde{p}}}(\bar{s}) + C_{l_{\dot{p}}}\bar{s}\right]\tilde{p} + \left[C_{l_{\tilde{r}}}(\bar{s}) + C_{l_{\dot{r}}}\bar{s}\right]\tilde{r} \tag{125}$$

$$C_n(\bar{s}) = \left[C_{n_{\tilde{\beta}}}(\bar{s}) + C_{n_{\dot{\beta}}}\bar{s}\right]\tilde{\beta} + \left[C_{n_{\tilde{p}}}(\bar{s}) + C_{n_{\dot{p}}}\bar{s}\right]\tilde{p} + \left[C_{n_{\tilde{r}}}(\bar{s}) + C_{n_{\dot{r}}}\bar{s}\right]\tilde{r} \tag{126}$$

The linearized equations of motion are then expressed in the nondimensional matrix form as

$$\mathbf{M}_{lat}(\bar{s})\,\bar{s}\mathbf{x}_{lat} = \mathbf{S}_{lat}(\bar{s})\,\mathbf{x}_{lat} \tag{127}$$

where $\mathbf{x}_{lat} = \begin{bmatrix} \tilde{\beta} & \tilde{p} & \tilde{r} & \tilde{\phi} \end{bmatrix}^\top$ is the nondimensional longitudinal aircraft state vector and the nondimensional reduced-frequency dependent matrices $\mathbf{M}_{lat}(\bar{s})$ and $\mathbf{S}_{lat}(\bar{s})$ are given by

$$\mathbf{M}_{lat}(\bar{s}) = \begin{bmatrix} \dfrac{2mV_\infty^2}{q_\infty Sb} - C_{Y_{\dot{\beta}}} & -C_{Y_{\dot{p}}} & -C_{Y_{\dot{r}}}\bar{s} & 0 \\ -C_{l_{\dot{\beta}}} & \dfrac{4I_{xx}V_\infty^2}{q_\infty Sb^3} - C_{l_{\dot{p}}} & -\dfrac{4I_{xz}V_\infty^2}{q_\infty Sb^3} - C_{l_{\dot{r}}} & 0 \\ -C_{n_{\dot{\beta}}} & -\dfrac{4I_{xz}V_\infty^2}{q_\infty Sb^3} - C_{n_{\dot{p}}} & \dfrac{4I_{zz}V_\infty^2}{q_\infty Sb^3} - C_{n_{\dot{r}}} & 0 \\ 0 & 0 & 0 & 1 \end{bmatrix} \tag{128}$$

$$\mathbf{S}_{lat}(\bar{s}) = \begin{bmatrix} C_{Y_{\tilde{\beta}}}(\bar{s}) & \dfrac{2mV_\infty^2}{q_\infty Sb}\bar{\alpha} + C_{Y_{\tilde{p}}}(\bar{s}) & -\dfrac{2mV_\infty^2}{q_\infty Sb} + C_{Y_{\tilde{r}}}(\bar{s}) & \dfrac{mg}{q_\infty S} \\ C_{l_{\tilde{\beta}}}(\bar{s}) & C_{l_{\tilde{p}}}(\bar{s}) & C_{l_{\tilde{r}}}(\bar{s}) & 0 \\ C_{n_{\tilde{\beta}}}(\bar{s}) & C_{n_{\tilde{p}}}(\bar{s}) & C_{n_{\tilde{r}}}(\bar{s}) & 0 \\ 0 & 1 & \bar{\theta} & 0 \end{bmatrix} \tag{129}$$

The eigenvalues of the lateral-directional flight dynamics can be computed as the zeros of the following transfer function matrix which are the roots of the characteristic equation

$$\left|\mathbf{M}_{lat}(\bar{s})\,\bar{s} - \mathbf{S}_{lat}(\bar{s})\right| = 0 \tag{130}$$

Figure 23 is the plot of the eigenvalues of the longitudinal flight dynamics of the Mach 0.8 TTBW. All the eigenvalues are stable. For comparison, the eigenvalues of the the longitudinal flight dynamics of the Mach 0.8 TTBW using the steady state stability derivatives by letting $\bar{s} = 0$ in all the dynamic stability derivatives are also computed and plotted. The frequencies and damping of the lateral-directional flight dynamic modes are listed in Table 2.

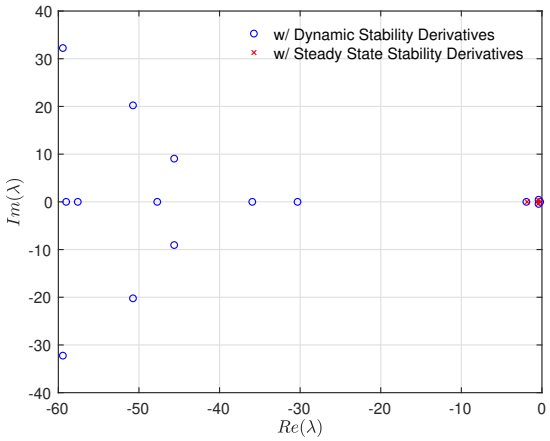

Figure 23. Eigenvalues of Longitudinal Flight Dynamics of Mach 0.8 TTBW

Mode	λ	ω (rad/sec)	ζ
Dutch Roll	$-0.4176 \pm i0.4370$	0.60444	0.6909
Roll	-1.9343	1.9343	1
Spiral	-0.2175	0.2175	1

(a) with Dynamic Stability Derivatives

Mode	λ	ω (rad/sec)	ζ
Dutch Roll	$-0.4427 \pm i0.3827$	0.5852	0.7565
Roll	-1.8295	1.8295	1
Spiral	-0.2349	0.2349	1

(b) with Steady State Stability Derivatives

Table 2. Lateral-Directional Flight Dynamic Modes

V. Conclusions

This paper presents a frequency-domain estimation of the dynamic stability derivatives of aircraft using high-fidelity CFD simulations. The unsteady aerodynamic coefficients due to the pitch motion are contributed by both the angle of attack and pitch rate. Similarly, the unsteady aerodynamic coefficients due to the yaw motion are contributed by both the angle of sideslip and yaw rate. The paper present an approach to obtain the pitch rate and yaw rate components from the aerodynamic coefficients by subtracting off the angle of attack and angle of sideslip contributions, respective. A method for estimating the dynamic stability derivatives for the unsteady drag coefficient is also presented in the paper. A complete set of dynamic stability derivatives of the Mach 0.8 Transonic Truss-Braced Wing have been obtained from a series of CFD simulations of forced oscillations in the axial airspeed, angle of attack, angle of sideslip, roll, pitch, and yaw. These derivatives are used to perform the flight dynamic analysis. The eigenvalues are obtained from the linearized equations of motion. The results show that all the aircraft flight dynamic modes are stable.

Acknowledgment

The authors wish to acknowledge NASA Advanced Air Transport Technology project for the funding support of this work. The authors also acknowledge Boeing Research and Technology and in particular Christopher Droney, Neal Harrison, Michael Beyar, Eric Dickey, and Anthony Sclafani, along with the NASA technical POC, Gregory Gatlin, for their research conducted under the NASA BAART contracts NNL10AA05B and NNL16AA04B. The research published in this paper is made possible by the technical data and wind tunnel test data furnished under these BAART contracts.

References

[1]Wang, F., and Chen, L., "Numerical Prediction of Stability Derivatives for Complex Configurations," Procedia Engineering 99 (2015) 1561-1575.

[2]Ghoreyshi M., Bergeron K., Lofthouse, A., and Cummings R., "CFD Calculation of Stability and Control Derivatives For Ram-Air Parachutes," AIAA Applied Aerodynamics Conference, AIAA-2016-1536, 2016.

[3]Murmann, S., "A Reduced-Frequency Approach for Calculating Dynamic Derivatives," AIAA Aerospace Sciences Meeting, AIAA-2005-0840, 2005.

[4]Nguyen, N. and Xiong, J., "CFD-Based Frequency Domain Method for Dynamic Stability Derivative Estimation with Application to Transonic Truss-Braced Wing," AIAA Aviation Forum, Applied Aerodynamics, AIAA-2022-3596, June 2022.

[5]Theodorsen, T., "General Theory of Aerodynamic Instability and the mechanism of Flutter", NACA Report No. 496, 1949.

[6]Bradley, M. K. and Droney, C. K., "Subsonic Ultra Green Aircraft Research: Phase I Final Report," NASA Contractor Report NASA/CR-2011-216847, Boeing Research and Technology, April 2011.

[7]Bradley, M. K., Droney, C. K., and Allen, T. J., "Subsonic Ultra Green Aircraft Research Phase II: N+4 Advanced Concept Development," NASA Contractor Report NASA/CR-2012-217556, Boeing Research and Technology, May 2012.

[8]Nguyen, N., Fugate, J., Kaul, U., and Xiong, J., "Flutter Analysis of the Transonic Truss-Braced Wing Aircraft Using Transonic Correction," AIAA Structural Dynamics Conference, AIAA-2019-0217, January 2019.

[9]Kaul, U. and Nguyen, N., "RANS Simulations of a Pitching and Plunging VCCTEF Airfoil Toward a Transonic Flutter Model," AIAA Structural Dynamics Conference, AIAA-2019-2037, January 2019.

[10]Kaul, U. and Nguyen, N., "Extending A Correction Method for Unsteady Transonic Aerodynamics as Applied to Variable Camber Continuous Trailing Edge Flap," AIAA Applied Aerodynamic Conference, AIAA-2019-3157, June 2019.

[11]Nguyen, N. and Xiong, J., "Transonic Correction to Theodorsen's Theory for Oscillating Airfoil in Pitch and Plunge Toward Flutter," AIAA Structural Dynamics Conference, AIAA-2021-1913, January 2021.

[12]Xiong, J. and Nguyen, N., "Steady and Unsteady Simulations of Transonic Truss-Braced Wing Aircraft for Flight Dynamic Stability Analysis," AIAA Applied Aerodynamics Conference, June 2022.

[13]Chaparro, D., Fujiwara, G. E., Ting, E., and Nguyen, N. T., "Transonic and Viscous Potential Flow Method Applied to Flexible Wing Transport Aircraft," 35th AIAA Applied Aerodynamics Conference, AIAA-2017-4221, June 2017.